# Development of the global maize yield model MATCRO-Maize version 1.0

Marin Nagata<sup>1</sup>, Astrid Yusara<sup>2</sup>, Tomomichi Kato<sup>3\*</sup>, Yuji Masutomi<sup>4</sup>

<sup>1</sup>Graduate School of Global Food Resources, Hokkaido University, Sapporo, Hokkaido 060-0809, Japan

<sup>2</sup>Graduate School of Agriculture, Hokkaido University, Sapporo, Hokkaido 060-0808, Japan

<sup>3</sup>Research Faculty of Agriculture, Hokkaido University, Sapporo, Hokkaido 060-8589, Japan

<sup>4</sup>Center for Climate Change Adaptation, National Institute for Environmental Studies, Tsukuba, Ibaraki 305-8506, Japan

Correspondence to: Tomomichi Kato (tkato@agr.hokudai.ac.jp)

**Abstract.** Process-based crop models combined with land surface models are useful tools for accurately quantifying the impacts of climate change on crops while considering the interactions between agricultural land and climate. MATCRO model is a process-based crop model initially developed for paddy rice, combined with a land surface model. We developed MATCRO-Maize as a new model for maize by incorporating leaf-level photosynthesis of C4 plants and adjusting crop-specific parameters into the original MATCRO model. MATCRO-Maize was evaluated at both a point scale and a global scale through comparisons with observational values. For global-scale simulations, the simulated yield showed statistically significant differences compared with Food and Agriculture Organization's FAOSTAT data at the country and global levels. Although the absolute value of the simulated yield tended to be overestimated, MATCRO-Maize reproduced spatial patterns with a correlation coefficient (COR) of 0.58 (p value < 0.01) for the 30-year average yield comparison of the top 20 maize-producing countries. In addition, the comparisons of the interannual variability derived from detrended deviation were statistically significant for the total global yield (COR of 0.55 with p value < 0.01) and for half of the top 20 countries (COR of 0.64-0.90 with p value < 0.001 for 6 countries; COR of 0.50-0.51 with p value < 0.01 for 2 countries; COR of 0.48-0.55 with p value <0.05 for 2 countries), which are comparable with those of other global crop models. One of the reasons for this overestimation could be related to the strong model response to nitrogen fertilizer observed in MATCRO-Maize. With experimental field data under more comprehensive conditions, improvements in the functions of nitrogen fertilizer in the model would be needed to simulate the maize yield more accurately.

#### 1 Introduction

Maize (*Zea mays* L.) is one of the most important cereals not only because of its large production (FAO, 2022) but also because of its various roles in human food, feed, and industrial uses. Maize exhibits high photosynthetic efficiency due to its C4 plant nature. It contains phosphoenolpyruvate (PEP) carboxylase in mesophyll cells, which concentrates CO<sub>2</sub> in bundle sheath cells. The concentrated CO<sub>2</sub> increases the relative amount of carboxylation versus oxygenation performed by ribulose-1,5-

bisphosphate carboxylase/oxygenase (Rubisco) (Kanai and Edwards, 1999), allowing C4 plants to operate at lower stomatal conductance rates than C3 plants (Sage, 1999). This mechanism results in high efficiencies of light, water, and nitrogen use (Knapp and Medina, 1999; Long, 1999). These features, such as multipurpose crops and high photosynthetic efficiency, enable the cultivated area to range over wide environments from wet to dry and from low to midlatitudes. However, climate change impacts and climate-related extremes negatively affect the productivity of the agricultural sector, which leads to negative consequences for food security (Intergovernmental Panel on Climate Change (IPCC), 2023). Therefore, it is important to accurately quantify the impact of climate change on crop growth and yield and to identify effective adaptation strategies to mitigate climate risk.

Process-based crop models are useful tools for climate change studies because they consider the response of the physiological processes of crop growth and development to the environment and management (Tubiello and Ewert, 2002). The ensemble of process-based crop model simulations has shown good agreement with observed maize yields both at the site scale and at the global scale (Bassu et al., 2014; Jägermeyr et al., 2021), showing its potential to quantify the uncertainty in studies on the impacts of climate change on crop yields (Asseng et al., 2013). Crop models combined with Land Surface Models (LSMs) or Earth System Models (ESMs) (as classified by Peng et al., 2017) have the ability to consider the effects of agricultural land on the climate globally through the exchange of fluxes of heat, water, and gases, as well as the effects of climate on crops. Some studies have revealed that agricultural land affects the climate through fluxes (Bondeau et al., 2007; Levis et al., 2012; Maruyama and Kuwagata, 2010; Tsvetsinskaya et al., 2001) and subsequently affects crop production (Osborne et al., 2009). This indicates the importance of considering the interaction between agricultural land and climate to accurately quantify the impacts of climate change on crops. Despite this importance, few LSM/ESM-based crop models exist (Lin et al., 2021; Lombardozzi et al., 2020; Osborne et al., 2015; Wu et al., 2016).

40

60

MATCRO is a process-based crop growth model developed for C3 plants (Masutomi et al., 2016a, b; Yusara et al., 2025). It was initially combined with a land surface model of Minimal Advanced Treatments of Surface Interaction and Runoff, called MATSIRO (Takata et al., 2003). MATSIRO is embedded in an ESM, which is the Model for Interdisciplinary Research on Climate, Earth System version 2 for Long-term simulations called MIROC-ES2L (Hajima et al., 2020). MATCRO simulates crop growth based on leaf-level photosynthesis and parameterized crop-specific parameters determined from experimental data, and it can run simulations both at a point scale and at a global scale. The model was applied to assess the impact of climate change at the country and local levels (Kinose et al., 2020; Kinose and Masutomi, 2019), and it was used in a study investigating factors to improve the simulation performance of global gridded crop models (GGCMs) (Iizumi et al., 2021). MATCRO is applicable to other crops, including maize as a C4 plant, with adjusted parameters from experimental datasets and the literature.

We extended MATCRO for global maize yield simulation, called MATCRO-Maize, by adjusting crop-specific parameters for maize and incorporating the C4 photosynthetic mechanism. The original model of MATCRO-Rice can simulate latent heat flux, sensible heat flux, net carbon uptake by crops, and rice yield, indicating its application in studies on climate change impacts as an LSM-based model (Masutomi et al. 2016b). However, this study focused only on crop growth and yields,

omitting water and heat fluxes to increase computational efficiency. This paper aims to describe the methodology of MATCRO-Maize in detail (Section 2), to evaluate simulated yields both at a point scale and at a global scale with reference datasets (Section 3), and to provide discussion of the evaluation and model limitations (Section 4).

## 2. Model description

MATCRO consists of four modules: radiation, net carbon assimilation, crop growth, and soil water balance. It requires the following input data: (i) phenological data (i.e., crop calendar), (ii) water management data (i.e., the land is rainfed or irrigated), (iii) nitrogen fertilizer application data ( $N_{fert}$ ) [kg N ha<sup>-1</sup>], (iv) soil classification data (i.e., soil texture classification), (v) annual CO<sub>2</sub> data [ppm], and (vi) 6 types of daily meteorological data: air pressure ( $P_s$ ) [Pa], precipitation ( $P_{rc}$ ) [kg m<sup>-2</sup> s<sup>-1</sup>], specific humidity [ $S_h$ ] [kg kg<sup>-1</sup>], downwards shortwave radiation ( $R_s$ ) [W m<sup>-2</sup>], maximum, minimum, and mean air temperature ( $T_{max}$ ,  $T_{min}$ ,  $T_a$ ) [K], and wind speed (U) [m s<sup>-1</sup>]. Based on input data, MATCRO simulates crop growth during a growing period. It is controlled by the crop developmental stage ( $D_{vs}$ ) based on (Bouman et al., 2001), which is the index used to quantify crop development. The final crop yield is determined by the dry weight of the storage organ with a parameter ( $K_{yld}$ ) when  $D_{vs} = 1$ . To adapt MATCRO for maize, crop-specific parameters and equations were improved, as shown in Table 1 and Eq. (1)–(35). The details are described in the following sections.

## 2.1 Photosynthetic mechanism

MATCRO-Maize calculates net carbon assimilation for the entire canopy  $(A_n)$  via the big-leaf model, where C4 leaf-level photosynthesis is separately calculated for sunlit and shaded leaves from the coupled photosynthesis–stomatal conductance model (Dai et al., 2004).

 $A_n$  for the entire canopy is given by:

$$A_n = \overline{A}_{n-sn} L_{sn} + \overline{A}_{n-sh} L_{sh}, \tag{1}$$

where  $\overline{A}_{n,sn}$  and  $\overline{A}_{n,sh}$  represent the net carbon assimilation per unit leaf area [ $\mu$  mol m<sup>-2</sup> s<sup>-1</sup>];  $L_{sn}$  and  $L_{sh}$  represent the leaf area index (LAI) [m<sup>2</sup> (leaf) m<sup>-2</sup>]; and sn and sh indicate sunlit and shaded leaves, respectively.  $\overline{A}_{n,sh}$  are defined in the following equations:

$$\overline{A}_{n,x} = \overline{A}_{g,x} - \overline{R}_{d,x},\tag{2}$$

where  $\overline{A}_{g,x}$  and  $\overline{R}_{d,x}$  represent gross carbon assimilation and dark respiration per unit leaf area [ $\mu$  mol m<sup>-2</sup> s<sup>-1</sup>], respectively.

Suffix x means sn or sh.  $L_{sn}$  and  $L_{sh}$  are determined following the approach of Masutomi et al., (2016a).  $\overline{R}_{d,x}$  is calculated via the following equation (Bonan et al., 2011):

$$\overline{R}_{d,x} = 0.025 V_{cmax,x} \left( \frac{2^{(Tv-298.15)/10}}{1 + \exp(1.3(Tv-328.15))} \right), \tag{3}$$

where  $V_{cmax,x}$  [ $\mu$  mol m<sup>-2</sup> s<sup>-1</sup>] is the maximum rate of carboxylation and where  $T_v$  is the leaf temperature [K] (assumed to be the same as the air temperature:  $T_a$ ).

95  $\overline{A}_{g,x}$  is determined by the smaller root of the following equations:

110

120

$$\beta_{cj}\overline{A}_{i,x}^2 - (\overline{A}_{c,x} + \overline{A}_{j,x})\overline{A}_{i,x} + \overline{A}_{c,x}\overline{A}_{j,x} = 0, \tag{4}$$

$$\beta_{ip}\overline{A}_{g,x}^2 - (\overline{A}_{i,x} + \overline{A}_{p,x})\overline{A}_{g,x} + \overline{A}_{i,x}\overline{A}_{p,x} = 0,$$
(5)

where  $\beta_{cj}$  and  $\beta_{ip}$  are the transition factors (Table 1) and where  $\overline{A}_{i,x}$  [ $\mu$  mol m<sup>-2</sup> s<sup>-1</sup>] is the carbon fixation rate. Here, we introduced the C4 leaf-level photosynthesis model based on Collatz et al. (1992) into MATCRO, in which some parameters were taken from Oleson et al., (2013) and Lawrence et al., (2020) (see Table 1). In C4 photosynthesis,  $\overline{A}_{c,x}$ ,  $\overline{A}_{j,x}$ , and  $\overline{A}_{p,x}$  [ $\mu$  mol m<sup>-2</sup> s<sup>-1</sup>] represent Rubisco-limited, RUBP-limited, and PEP-limited photosynthesis, respectively, and are given by the following equations:

$$\overline{A}_{cx} = V_{cmax} \,, \tag{6}$$

$$\overline{A}_{j,x} = \alpha(4.6Q_{ab,x}),\tag{7}$$

105 
$$\overline{A}_{p,x} = k_{p,x} C_{i,x}$$
, (8)

where  $Q_{ab,x}$  [W m<sup>-2</sup>] is the absorbed photosynthetically active radiation (PAR);  $\alpha$  [mol mol<sup>-1</sup>] is the quantum efficiency;  $k_{p,x}$  [mol m<sup>-2</sup> s<sup>-1</sup>] is the initial slope of the CO<sub>2</sub> response curve for the C4 CO<sub>2</sub> response curve; and  $C_{i,x}$  [ppm] is the internal leaf CO<sub>2</sub> concentration.  $Q_{ab,x}$  is calculated from  $R_s$  via the same methods conducted in Masutomi et al. (2016a) and is converted to photosynthetic photon flux by multiplying by 4.6 [ $\mu$  mol (photons) J<sup>-1</sup>].  $V_{cmax,x}$  and  $k_{p,x}$  are functions of  $T_v$  and are based on Lawrence et al. (2020),

$$V_{cmax,x} = f_v V_{cmax25,x} \left[ \frac{\varrho_{10}^{(T_v - 298.15)/10}}{f_H(T_v)f_L(T_v)} \right], \tag{9}$$

$$f_H(T_v) = 1 + \exp[S_1(T_v - S_2)],\tag{10}$$

$$f_L(T_v) = 1 + \exp[S_3(S_4 - T_v)],\tag{11}$$

$$k_{p,x} = \begin{cases} k_{p25,x} Q_{10}^{(T_v - 298.15)/10}, & V_{cmax25,x} > 0, \\ 0.7, & V_{cmax25,x} = 0, \end{cases}$$
(12)

$$115 \quad k_{p25,x} = 20000V_{cmax25,x} \,, \tag{13}$$

with  $Q_{10} = 2$ ,  $S_1 = 0.3 \, K^{-1}$ ,  $S_2 = 313.15 K$ ,  $S_3 = 0.2 \, K^{-1}$ , and  $S_4 = 288.15 K$  (see Table 1). Notably,  $k_{p,x}$  is adjusted to be 0.7  $mol \ m^{-2} \ s^{-1}$  (Collatz et al., 1992) when  $V_{cmax25,x} = 0$  because of the process of the photosynthesis calculation (see Eq. (20)).  $V_{cmax25,x}$  is the maximum Rubisco carboxylation rate per unit leaf area at 25°C (the details are described in Section 2.2.2).  $f_H(T_v)$  and  $f_L(T_v)$  are modulating functions that reduce  $V_{cmax,x}$  at high and low temperatures, respectively.  $f_v$  is the water stress factor calculated in the soil water balance module, which indirectly affects  $A_n$  through  $V_{cmax,x}$  (Sellers et al., 1996).  $f_v$  is derived from the following equations:

$$f_{v} = \sum_{i=1}^{NSL} \left\{ \frac{1 * ETF(i), FAW(i) > 0.45,}{\frac{FAW(i)}{0.45} * ETF(i), otherwise,} \right\}$$
(14)

$$FAW(i) = \min\left(\frac{\max(WSL(i) - WILT), 0)}{FC - WILT}, 1\right),\tag{15}$$

$$ETF(i) = \frac{3}{2} \frac{(z_{rt}^2 - z^2)}{z_{rt}^3},\tag{16}$$

- where *NSL* represents the number of soil layers, *ETF* represents the fraction of transpiration from root distribution, *FAW* represents the fraction of available water, *WSL* represents the soil water content [m³ m⁻³], *WILT* represents the wilting point, *FC* represents the field capacity, and  $z_{rt}$  and z represent the root depth and the soil depth, respectively, for each layer. MATCRO assumes NSL = 5, where each of the soil layers has depth of 0.05, 0.2, 0.75, 1, and 2 [m] below the ground, respectively. MATCRO uses the soil texture data as input data, where the soil is classified into 13 types, leading to differences in *WILT* and *FC* based on Campbell and Norman (1998). *WSL* is calculated considering transpiration from the canopy, evaporation from the soil, and water flux (those calculations are the same as those of the original MATCRO). The *ETF* calculation assumes that the root has no spatial orientation and is equally distributed in the soil (Masutomi et al., 2016a).  $z_{rt}$  is determined by the same calculation as the original MATCRO, where the crop-specific parameter ( $z_{rt,mx}$ ) was changed to maize (Table 1). The conditional branch (*FAW* (*i*) > 0.45) is based on the FAO 56 guidelines (Allen et al., 1998).
- Stomatal conductance influences CO<sub>2</sub> uptake during photosynthesis. MATCRO-Maize represents stomatal conductance for CO<sub>2</sub> ( $G_{sc,x}$  [ $\mu$  mol m<sup>-2</sup> s<sup>-1</sup>]), based on Ball (1988) as follows:

$$G_{sc,x} = \begin{cases} G_{0c} + G_{1c}R_h \frac{\overline{A}_{n,x}}{c_{s,x}}, \ \overline{A}_{n,x} \ge 0, \\ G_{0c}, \ otherwise, \end{cases}$$

$$(17)$$

where  $C_{s,x}$  [ppm] is the CO<sub>2</sub> concentration at the leaf surface and  $R_h$  [-] is the relative humidity at the leaf surface.  $G_{0c}$  and  $G_{1c}$  are derived from parameters of Ball-Berry stomatal conductance model of b and m (shown in Table 1) by adjusting their ratio of 1:1.6, which is the ratio of diffusivity of H<sub>2</sub>O to CO<sub>2</sub>. Here, the leaf-level net carbon assimilation rate  $(\overline{A}_{n,x})$ , stomatal conductance for CO<sub>2</sub>  $(G_{sc,x})$ , and boundary layer conductance for CO<sub>2</sub>  $(G_{bc})$  were calculated to satisfy the following physical flux equations.

140

150

$$\overline{A}_{n,x} = G_{sc,x}(C_{s,x} - C_{i,x}),\tag{18}$$

$$\overline{A}_{n,x} = G_{bc} \left( C_a - C_{s,x} \right), \tag{19}$$

where  $C_a$  [ppm] is the atmospheric CO<sub>2</sub> concentration.  $G_{bc}$  is a function of air pressure ( $P_s$  [Pa]) and the wind speed in the canopy (U [m s<sup>-1</sup>]).

Here,  $T_v$ ,  $Q_{ab,x}$ ,  $R_h$ , U, and  $C_a$  are environmental variables derived from input meteorological climate data. There are four relationships (Eqs. (2), (17)-(19)) in terms of internal variables ( $\overline{A}_{n,x}$ ,  $G_{sc,x}$ ,  $C_{s,x}$ ,  $C_{i,x}$ ). MATCRO for C3 photosynthesis obtains analytical solutions from relationships via the method shown in Masutomi (2023). For C4 photosynthesis, it is also possible to solve these equations analytically. In the case of Rubisco-limited and RuBP-limited photosynthesis, exact expressions for  $\overline{A}_{c,x}$ 

and  $\overline{A}_{j,x}$  are obtained. Under  $\overline{A}_{n,x} \ge 0$ , PEP-limited photosynthesis  $(\overline{A}_{p,x})$  can be represented by quadratic equations by the algebraic procedures as follows:

$$0 = \left\{ G_{bc}^2 G_{1c} R_h - G_{bc} G_{0c} - k_{p,x} (G_{0c} - G_{bc} G_{1c} R_h + G_{bc}) \right\} \bar{A}_{p,x}^2 + \left\{ C_a G_{bc}^2 G_{0c} - G_{bc} G_{0c} R_d + G_{bc}^2 G_{1c} R_h R_d - k_{p,x} C_a (G_{bc}^2 G_{1c} R_h - 2G_{bc} G_{0c} - G_{bc}^2) \right\} \bar{A}_{p,x} + C_a G_{bc}^2 G_{0c} (R_d - k_{p,x} C_a).$$

$$(20)$$

Under  $\overline{A}_{n,x}$  < 0, the PEP-limited photosynthesis rate can be expressed as

$$\bar{A}_{p,x} = \frac{k_{p,x} c_a - R_d}{1 + k_{p,x} \left(\frac{1}{G_{bc}} + \frac{1}{G_{0c}}\right)}.$$
(21)

According to these equations, in the case of PEP-limited photosynthesis, there are three possible solutions. Following the criteria described by Masutomi (2023), only one analytical solution can be selected when the following requirements are satisfied: (i) under  $\overline{A}_{n,x} \ge 0$ , the solution must be a positive or zero real solution, and under  $\overline{A}_{n,x} < 0$ , it must be a negative real solution; (ii)  $G_{sc.x} > 0$ ; and (iii)  $C_i > 0$ .

# 2.2 Crop-specific parameterization

# 2.2.1 Phenology

160

The crop growing period in MATCRO is expressed as  $D_{vs}$  based on Bouman et al. (2001). Here,  $D_{vs} = 0$  means sowing, and  $D_{vs} = 1$  means maturity (harvesting). It is calculated from the following equations:

165 
$$D_{vs,i} = G_{dd,i}/G_{ddm,i},$$
 (22)

$$G_{dd} = \int_0^t D_{vr} dt', \qquad (23)$$

$$D_{vr} = \begin{cases} 0, \ T_t < T_b \mid T_h \le T_t, \\ T_t - T_b, \ T_b \le T_t < T_o, \\ \frac{(T_b - T_o)(T_t - T_h)}{(T_h - T_o)}, \ T_o \le T_t < T_h, \end{cases}$$
(24)

where  $G_{dd,i}$  is the growing degree days at t (time) for specific grid cell number i;  $G_{ddm,i}$  is the growing degree day at maturity;  $D_{vr}$  is the developmental rate at time t; and  $T_t$  is the temperature at time t.  $T_b$ ,  $T_h$ , and  $T_o$  are the crop-specific cardinal temperatures (minimum, maximum, and optimal temperatures for development, respectively, as shown in Table 1).  $G_{dd,m}$  were calibrated for each point scale simulation and global scale simulation (Section 2.3). In addition, one parameter that represents the timing of flowering (known as silking;  $D_{vs,flw}$ ) was calibrated based on observational data for the point scale simulation (Table 1).

# 2.2.2 Leaf nitrogen and Rubisco capacity

## 175 Maximum Rubisco carboxylation rate

 $V_{cmax25,x}$  used in the photosynthesis module (Section 2.1) is obtained by dividing the maximum Rubisco carboxylation rate at a LAI depth of l ( $V_{cmax25,x}(l)$ ) by  $L_x$  separately for sunlit and shaded leaves based on Bonan et al. (2011). The vertical distribution of  $V_{cmax25}(l)$ , which is the sum of  $V_{cmax25,sn}(l)$  and  $V_{cmax25,sh}(l)$ , follows the exponential profile:

$$V_{cmax25}(l) = V_{cmax25}(0) \exp(-K_n l), \tag{25}$$

where  $V_{cmax25}(0)$  is the maximum Rubisco carboxylation rate at the canopy top,  $K_n$  is a parameter for the vertical distribution of nitrogen (Table 1), and l represents the LAI depth from the top. The maximum Rubisco carboxylation rate in sunlit leaves  $(V_{cmax25.sn}(l))$  is also calculated by the same relationship considering the light distribution:

$$V_{cmax25,sn}(l) = V_{cmax25}(0)[1 - exp(-l(K_n + K))] \frac{1}{K_n + K},$$
(26)

where K is the direct beam extinction coefficient (the calculation is the same as that for Masutomi et al., 2016a).  $V_{cmax25,sh}(l)$  is given by the subtraction of Eq. (25) and Eq. (26).

Here, while Bonan et al. (2011) use the fixed value of  $V_{cmax25}(0)$  value over time,  $V_{cmax25}(0)$  in MATCRO is calculated dynamically as a function of specific leaf nitrogen ( $S_{ln}$  [g N m<sup>-2</sup>]). The function is established based on the experimental literature data. Notably, we applied the relationship between  $S_{ln}$  and light-saturated CO<sub>2</sub> assimilation ( $A_{max}$ ) from the literature, although MATCRO-Rice and MATCRO-Soy utilize the direct relationship between  $S_{ln}$  and  $V_{cmax25}(0)$  based on the experimental literature data. The reasons are that we assume that  $A_{max}$  could be used as Rubisco-limited photosynthesis in C4 photosynthesis, hence Rubisco-limited photosynthesis could be equal to the maximum Rubisco carboxylation rate from Eq. (6). Several studies have shown that  $A_{max}$  has a close relationship with  $S_{ln}$ , as shown by the logistic equation for maize (Drouet and Bonhomme, 2004; Muchow and Sinclair, 1994; Paponov and Engels, 2003; Paponov et al., 2005; Sinclair and Horie, 1989; Vos et al., 2005). We used two functions from the studies for different  $D_{vs}$  as follows:

195 
$$V_{cmax25}(0) = \begin{cases} 45.1 * \left\{ \frac{2}{1 + \exp[-2.9 * (S_{ln} - 0.25)]} - 1 \right\}, \ D_{vs} < D_{vs,flw}, \\ 40.2 * \left\{ \frac{2}{1 + \exp[-1.41 * (S_{ln} - 0.43)]} - 1 \right\}, \ otherwise, \end{cases}$$
 (27)

where  $D_{vs} < D_{vs,flw}$  represents the vegetative stage at which the equation was based on Vos et al. (2005); then, for the reproductive stage, the equation was from Drouet and Bonhomme (2004). Stage-specific parameterizations were applied to reflect the lower photosynthetic activity observed during the reproductive phase compared to the vegetative phase since no single dataset adequately represents both growth phase.

# Specific leaf nitrogen

185

190

200

205

 $S_{ln}$ , which is used in the calculation of  $V_{cmax25}(0)$ , is dynamically change during the crop growth of  $D_{vs}$  in MATCRO. The function is established based on the observational data. We utilized the study by Muchow (1988), in which  $S_{ln}$  was measured under various levels of  $N_{fert}$  (0, 60, 120, 240, 420 [kg ha<sup>-1</sup>]), as follows: (i) we traced  $S_{ln}$  data using digitizer software (https://apps.automeris.io/wpd4/) and obtained the measurement and phenological data from the paper; and (ii) we conducted

the fitting based on the assumption that  $S_{ln}$  linearly increased until flowering and then decreased towards maturity. The parameterization given by Eqs. (28)–(30) is shown in Figure 1.

$$S_{ln} = \begin{cases} \frac{S_{ln,mx} - S_{ln,plt}}{D_{vs,flw}} D_{vs} + S_{ln,plt}, & D_{vs} < D_{vs,flw}, \\ \frac{S_{ln,matu} - S_{ln,mx}}{1 - D_{vs,flw}} (D_{vs} - 1) + S_{ln,matu}, & D_{vs} \ge D_{vs,flw}. \end{cases}$$
(28)

Where  $S_{ln,mx}$ ,  $S_{ln,nlt}$ ,  $S_{ln,matu}$  are maximum  $S_{ln}$ , and  $S_{ln}$  at planting time and maturity, respectively.  $S_{ln,nlt}$  was parameterized by assuming low  $S_{ln}$  in the early stage (Table 1). Menwhile,  $S_{ln,mx}$  and  $S_{ln,matu}$  are empirically parameterized as functions of 210  $N_{fert}$  as follows:

$$S_{ln,mx} = \begin{cases} -0.00001 N_{fert}^{2} + 0.0064 N_{fert} + 0.6891, & N_{fert} \le 240, \\ 1.75, & N_{fert} > 240. \end{cases}$$

$$S_{ln,mx} = \begin{cases} 0.001 N_{fert} + 0.57, & N_{fert} \le 240, \\ 0.001 N_{fert} + 0.57, & N_{fert} \le 240, \end{cases}$$

$$(29)$$

$$S_{ln,matu} = \begin{cases} 0.001 \, N_{fert} + 0.57, \ N_{fert} \le 240, \\ 1, \ N_{fert} > 240. \end{cases}$$
 (30)

We set fixed values of 1.75 for  $S_{ln,mx}$  and 1.0 for  $S_{ln,matu}$  when  $N_{fert}$  exceeds 240 [kg ha<sup>-1</sup>], as  $S_{ln,mx}$  and  $S_{ln,matu}$  exhibit 215 minimal increases beyond this threshold.

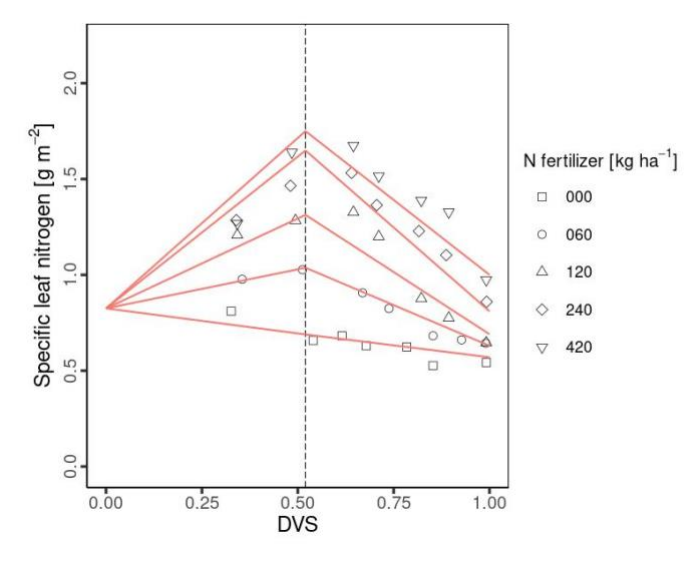


Figure 1. Relationship between developmental stage  $(D_{vs})$  and specific leaf nitrogen  $(S_{ln})$  in MATCRO-Maize. Symbols show observational data from Muchow (1988) with the 5 types of  $N_{fert}$ : 0 kg ha<sup>-1</sup> (square), 60 kg ha<sup>-1</sup> (cycle), 120 kg ha<sup>-1</sup> (triangle), 240 kg ha<sup>-1</sup> (diamond), and 420 kg ha-1 (inverted triangle). The red lines represent the fitted line parameters used in MATCRO-Maize, while the dashed line represents  $D_{vs}$  at flowering  $(D_{flw})$ .

#### 2.2.3 Crop growth

220

#### Glucose partitioning

MATCRO calculates crop growth by partitioning net carbon assimilation  $(A_n)$  in the form of glucose, which is calculated in the photosynthesis module (Section 2.1). Partitioned glucose is supplied through photosynthesis in leaves and remobilization from the stem. The ratio of glucose partition to each organ (leaf, stem, root, and storage organ; ear) depends on  $D_{vs}$ . The term "ear" in maize represents the organ that supports the development and storage of grain. The grain developed later than the ear with approximately 83% of ear at maturity in this study (see Section 2.2.5). The dry matter for each organ is obtained from the partitioned glucose considering the carbon fraction for each organ ( $C_{glu,ear}$ ,  $C_{glu,leaf}$ ,  $C_{glu,rot}$ ,  $C_{glu,stm}$  in Table 1). We calibrated the partitioning ratio to leaf and ear based on the observational biomass data from Ciampitti et al. (2013a, b), whereas the ratio to shoots:roots was derived from the value from Penning de Vries et al. (1989). The stem partitioning was determined by reducing the shoot ratio with respect to the leaf and ear. Figure 2 shows the partition ratio to the leaf ( $P_{r,lef}$ ) and ear ( $P_{r,ear}$ ) established via the following equations:

$$P_{r,lef} = \begin{cases} P_{lef}, D_{vs} < D_{vs,lef1}, \\ \frac{P_{lef}(D_{vs,lef2} - D_{vs})}{D_{vs,lef2} - D_{vs,lef2}}, D_{vs} < D_{vs,lef2}, \\ 0, otherwise, \end{cases}$$
(31)

$$P_{r,ear} = \begin{cases} 0, \ D_{vs} < D_{vs,ear1}, \\ \frac{D_{vs} - D_{vs,ear1}}{D_{vs,ear2} - D_{vs,ear1}}, \ D_{vs} < D_{vs,lef2}, \\ 1, \ otherwise, \end{cases}$$
(32)

where  $D_{vs,lef1}$ ,  $D_{vs,lef2}$ ,  $D_{vs,ear1}$  and  $D_{vs,ear2}$  represent the  $D_{vs}$  at which the corresponding partition changes, as described in Table 1 and based on Figure 2;  $P_{lef}$  is the ratio of glucose partitioned to glucose to the leaf from glucose partitioned to the shoot.

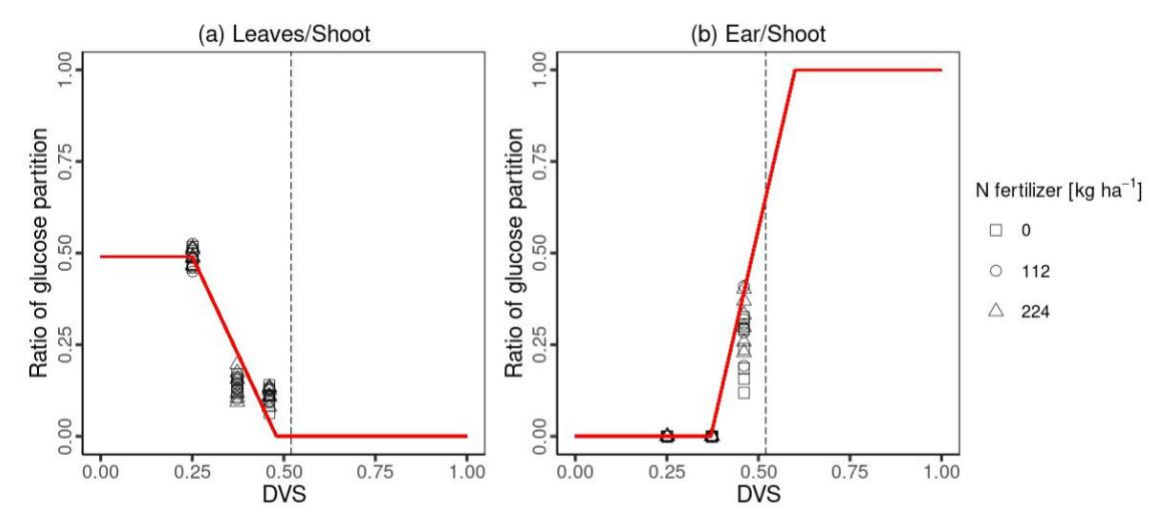


Figure 2. The ratio of glucose partitioning to leaves (a) and ears (b). Symbols show the ratio of glucose partition with different  $N_{fert}$ : 0 kg ha<sup>-1</sup> (square), 112 kg ha<sup>-1</sup> (cycle), and 224 kg ha<sup>-1</sup> (triangle) measured in Ciampitti et al. (2013a, b). The red lines in Figure 2 show the segmented line parameters used in MATCRO-Maize, while the dashed line represents  $D_{vs}$  at flowering ( $D_{vs,flw}$ ).

## Specific leaf weight

The specific leaf weight  $(S_{lw})$  is used to calculate the total leaf area index (L) in MATCRO. It is varied dynamically with the developmental stage of  $D_{vs}$  and is given by:

245  $S_{lw} = S_{lw,mx} + (S_{lw,mn} - S_{lw,mx}) \exp(-k_{Slw} D_{vs})$  (33)

where  $S_{lw,mn}$ ,  $S_{lw,mx}$ , and  $k_{Slw}$  are minimum, maximum, and absolute value of the rate constant in the  $S_{lw}$  function, respectively. These crop-specific parameters were derived from the observational data expressed in Table 1. We conducted curve fitting of  $S_{lw}$  to calculate the dry weight of the leaf biomass and the leaf area index based on Ciampitti et al. (2013a, b) and established a relationship (Figure 3).

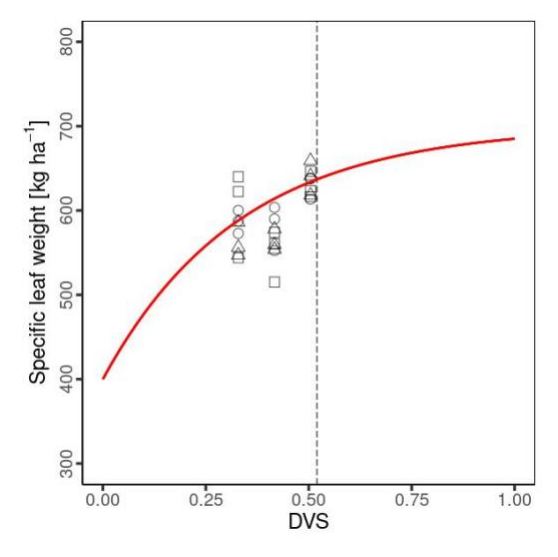


Figure 3. Relationships between specific leaf weights and developmental stages. Symbols are the same as in Fig. 2.

## 2.2.4 Crop height

250

Crop height  $(H_{gt})$  is related to the calculation of evapotranspiration in MATCRO. It assumes that the dependence of the crop height is based on  $D_{vs}$  using function from Penning de Vries et al. (1989) and is given by

255 
$$H_{gt} = \begin{cases} h_{aa} D_{vs} / D_{vs,flw}, & D_{vs} < D_{vs,flw} \\ h_{aa}, & D_{vs} \ge D_{vs,flw} \end{cases}$$
 (34)

where  $h_{aa}$  is the crop height at flowering (Table 1).

# 2.2.5 Crop yield

MATCRO calculates the final crop yield,  $Y_{ld}$ , from the dry weight of the storage organ at maturity ( $W_{ear,mt}$ ) as follows:

$$Y_{ld} = k_{yld} W_{ear,mt}. (35)$$

Here,  $k_{yld}$  is the crop-specific parameter (Table 1), which represents the ratio of  $Y_{ld}$  to  $W_{ear,mt}$ . The dry weight of the ear is a consistent predictor of the plant's potential yield at maturity. We parameterized  $K_{yld}$  using experimental data from Ciampitti et al. (2013b).

Variable	Value	Units	Description	Source
Crop-specific	(maize)			
b	0.04	mol (H <sub>2</sub> O) m <sup>-2</sup> s <sup>-1</sup>	intercept of the Ball-Berry model	Sellers et al. (1996)
$C_{glu,ear}$	0.815	ratio	conversion factor of dry weight from glucose to ear	Penning de Vries et al. (1989)
$C_{glu,leaf}$	0.871	ratio	conversion factor of dry weight from glucose to leaf	Penning de Vries et al. (1989)
$C_{glu,rot}$	0.857	ratio	conversion factor of dry weight from glucose to root	Penning de Vries et al. (1989)
$C_{glu,stm}$	0.810	ratio	conversion factor of dry weight from glucose to stem	Penning de Vries et al. (1989)
$D_{vs,rot1}$	0.35	ratio	1st point of $D_{vs}$ at which the partition pattern to root changes	Penning de Vries et al. (1989)
Crop-specific	(maize)			
$D_{vs,rot2}$	0.72	ratio	2nd point of $D_{vs}$ at which the partition pattern to root changes	Penning de Vries et al. (1989)
$D_{vs,ear1}$	0.37	ratio	1st point of $D_{vs}$ at which the partition pattern to ear changes	Parameterized in this study
$D_{vs,ear2}$	0.6	ratio	2nd point of $D_{vs}$ at which the partition pattern to ear changes	Parameterized in this study
$D_{vs,flw}$	0.52	ratio	$D_{vs}$ at flowering	Parameterized in this study
$D_{vs,lef1}$	0.25	ratio	1st point of $D_{vs}$ at which the partition pattern to leaf changes	Parameterized in this study
$D_{vs,lef2}$	0.48	ratio	2nd point of $D_{vs}$ at which the partition pattern to leaf changes	Parameterized in this study
$f_{stc}$	0.35	ratio	fraction of glucose allocated to starch reserves	Penning de Vries et al. (1989)
$h_{aa}$	2	m	crop height at flowering	Penning de Vries et al. (1989)
$k_{yld}$	0.83	ratio	ratio of crop yield to dry weight of ear at maturity	Parameterized in this study
$k_{Slw}$	3	ratio	parameter that represents the relationship between $S_{lw}$ and $D_{vs}$	Parameterized in this study
m	4	ratio	the slope of the Ball-Berry model	Sellers et al. (1996)
$G_{dd,m}$	_	K day	growing degree day at maturity	Parameterized in this study
$P_{lef}$	0.49	ratio	partition ratio of glucose to leaf from glucose partitioned to the shoot	Parameterized in this study
$P_{rot}$	0.25	ratio	partition ratio of glucose to root	Penning de Vries et al. (1989)
$r_{dl,lef}$	3.0×10 <sup>-7</sup>	$s^{-1}$	ratio of dead leaf at harvest	Masutomi et al. (2016)
$r_{rt}$	0.06	m s <sup>-1</sup>	growth ratio of root	Penning de Vries et al. (1989)
$S_{ln,plt}$	0.825	g m <sup>-2</sup>	specific leaf nitrogen at planting	Parameterized in this study
$S_{ln,mx}$	See Eq. (29)	g m <sup>-2</sup>	maximum specific leaf nitrogen	Parameterized in this study
$S_{ln,matu}$	See Eq. (30)	g m <sup>-2</sup>	specific leaf nitrogen at maturity	Parameterized in this study
$S_{lw,mn}$	400	kg ha <sup>-1</sup>	minimum specific leaf weight	Parameterized in this study
$S_{lw,mx}$	700	kg ha <sup>-1</sup>	maximum specific leaf weight	Parameterized in this study
$T_b$	8.6	°C	minimum temperature for development	Osborne et al. (2015)
$T_h$	42.0	°C	maximum temperature for development	Osborne et al. (2015)
$T_o$	30.0	°C	optimal temperature for development	Osborne et al. (2015)
$Z_{rt,mx}$	1.5	m	maximum root depth	Penning de Vries et al. (1989)
α	0.05	mol mol <sup>-1</sup>	quantum efficiency	Sellers et al. (1996)
$\beta_{cj}$	0.8	ratio	GPP transition factor	Lawrence et al. (2020)
Others				
$k_n$	0.3	ratio	vertical distribution of nitrogen	Oleson et al. (2013)
$S_1$	0.3	K-1	temperature dependence of $V_{cmax,x}$	Lawrence et al. (2020)
$S_2$	313.15	K	temperature dependence of $V_{cmax,x}$	Lawrence et al. (2020)
$S_3$	0.2	$K^{-1}$	temperature dependence of $V_{cmax,x}$	Lawrence et al. (2020)

Variable	Value	Units	Description	Source
$S_4$	288.15	K	temperature dependence of $V_{cmax,x}$	Lawrence et al. (2020)
$eta_{ip}$	0.95	ratio	GPP transition factor	Lawrence et al. (2020)

#### 2.3 Model evaluation

270

275

MATCRO can run the simulation both at a point scale and at a global scale. The developed model was evaluated both at a point scale and at a global scale. For point scale levels, LAI and total aboveground were compared with the observation data from the four sites. Meanwhile, we use yield data for evaluation. After confirming the ability of the model to simulate maize growth, two types of evaluations were conducted at the global scale. First, the simulated yields at the grid cell were compared with the gridded yield datasets of the Global Dataset of Historical Yields (GDHY; Iizumi and Sakai, 2020), GlobalCropYield (GCY; Cao et al., 2025), and the Spatial Production Allocation Model (SPAM; IFPRI, 2019). Second, the simulated yields at the country and total global levels were compared with the country yield report and global data from the Food and Agriculture Organization's FAOSTAT database (FAOSTAT, 2024). To quantify the model performance, four statistical values were used in this study: the Pearson correlation coefficient (COR), root mean square error (RMSE), relative root mean square error (RRMSE) and normalized mean absolute error (NMAE). RRMSE and NMAE were calculated as follows:

$$RMSE = \sqrt{\frac{1}{n} \sum_{i=1}^{n} (y_i - \hat{y}_i)^2},$$
(36)

$$RRMSE = \frac{RMSE}{\overline{y}},\tag{37}$$

$$NMAE = \frac{1}{n} \sum_{i=1}^{n} \frac{|\hat{y}_i - y_i|}{y_i},\tag{38}$$

280 where  $y_i$  is the actual value,  $\hat{y}_i$  is the predicted value, and  $\overline{y}$  is the mean of the actual value.

## 2.3.1 Model evaluation at a point scale

To evaluate the model performance at a field scale, we used observational data from four sites (Brazil, France, Tanzania, and the USA; Table 2) used in the Agricultural Model Intercomparison and Improvement Project (AgMIP) study (Bassu et al., 2014). We used local daily climate data of precipitation, downwards shortwave radiation, air temperature, wind speed ( $P_{rc}$ ,  $R_s$ ,  $T_a$ , U respectively), management data ( $N_{fert}$  and irrigation regime) and phenological data (planting, flowering, and maturity dates) for model input data at each site. We identified the soil texture from the gridded soil texture dataset of ISIMIP (Volkholz and Müller, 2020), and annual  $CO_2$  data from the ISIMIP3a (Büchner and Reyer, 2022). Climatic data were obtained from the NASA Modern Era Retrospective-Analysis for Research and Applications corrected with observational datasets (AgMERRA; Ruane et al., 2015) when measured data were unavailable (Bassu et al., 2014).

**Table 2.** Evaluation site information in the point-scale simulation

Country	Site	Latitude	Longitude	Soil type	Sowing date	Hybrid	Total N fertilizer [kg N ha <sup>-1</sup> ]	Irrigation
Brazil	Rio Verde	17.52°S	51.43°W	Geri-Gibbsic Ferralsol	Oct. 22nd 2003	Pioneer 30K75	0	No

France	Lusignan	46.25°N	00.07°E	Cambisol	Apr. 26th 1996	Furio	255	Yes
Tanzania	Morogoro	06.50°S	37.39°E	Haplic Arenosol	Oct. 26th 2009	TMV1	61	Yes
USA	Iowa	42.01°N	93.45°W	Gleysols	May 4th 2010	Golden Harvest GH-9014	167	No

Notably, air pressure  $(P_s)$  and specific humidity  $(S_h)$  data were not provided. Hence, we represented the point scale by extracting  $P_s$  from the nearest  $0.5^{\circ} \times 0.5^{\circ}$  grid cell of GSWP3-W5E5 dataset for the ISIMIP3a (Lange et al., 2022). Meanwhile,  $S_h$  was converted from  $R_h$  using  $T_a$  and the vapour pressure. We parameterized  $G_{dd,m}$  and  $D_{vs,flw}$  based on  $T_a$  and phenological data (sowing, flowering, and maturity dates).  $G_{dd,m}$  calibrated for each site is used for the simulations, while the average  $D_{vs,flw}$  over the 4 sites is used (0.52 in Table 1). As a result, the mean average errors were estimated as 4.25 and 7 days for flowering and maturity, respectively (Figure 4). MATCRO was run with these parameters, and then the model output was evaluated with the observations for the following 3 variables: seasonal change in the LAI, total aboveground biomass, and final yield.

295

310

Model calibration was conducted based on phenological data (Table 2, Bassu et al., 2014) and biomass data for carbon partitioning of leaves and ear (Figure 2, derived from Ciampitti et al., 2013a, b). In this study, a global parameter was applied uniformly across all regions at the grid-cell level instead of using site-specific calibrated parameters in the simulations. The model was then assessed at the point scale to verify calibration for phenology (flowering and maturity) and was evaluated against time-series data of LAI, aboveground biomass, and harvested yield (see Section 3.1), which were not included in the model calibration.

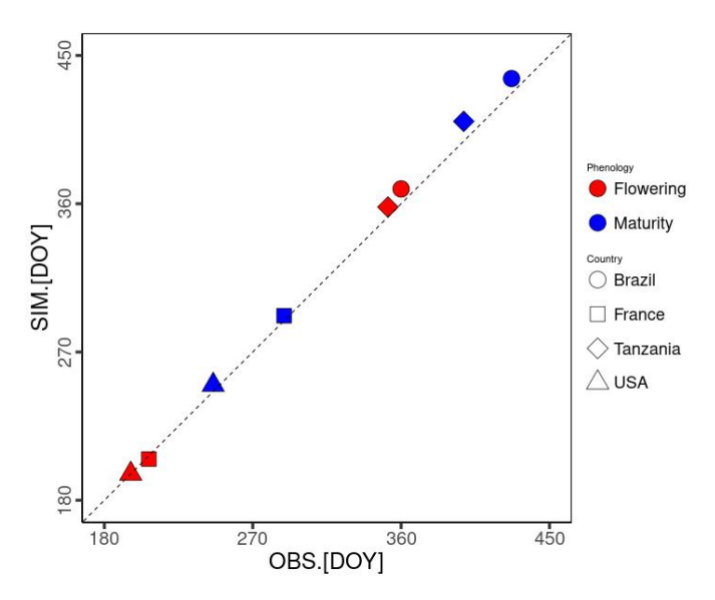


**Figure 4.** Model-fit comparison of the flowering and maturity date simulations (SIM on the y-axis) and observations (OBS on the x-axis). DOY represents the number of days from January 1<sup>st</sup>. Symbols show each site: Brazil (square), France (circle), Tanzania (triangle), and the USA (diamond). The colours indicate the phenological stages of flowering (red) and maturity (blue).

## 2.3.2 Model evaluation at a global scale

# **Simulation settings**

315

320

325

330

335

340

For the global-scale simulation, the model was run at a spatial resolution of  $0.5^{\circ} \times 0.5^{\circ}$  from 1980–2010 under both rainfed and irrigated conditions. The required input data were as follows. (i) Crop calendar data were from the Global Gridded Crop Model Intercomparison (GGCMI) phase 3 protocol (Jägermeyr et al., 2021). It provides planting and maturity dates for 18 different crops, including maize, separated by rainfed and irrigated systems. We parameterized the average  $G_{dd,m}$  at each grid over the period 1980-2010 for the growing season from the planting to maturity dates for each of the rainfed and irrigated conditions. Both the planting date and the simulated  $G_{dd,m}$  were used as the input data for the global-scale simulations. (ii) Water management data (i.e., irrigation regime) from the MIRCA2000 dataset (Portmann et al., 2010). In the case of irrigated conditions, the soil moisture was set to field capacity during the growing season. (iii)  $N_{fert}$  from the Inter-Sectoral Impact Model Intercomparison Project (ISIMIP; Volkholz and Ostberg, 2022). It provides the annual nitrogen fertilizer inputs for five canonical crop types, including C4 annual crops for maize. (iv) Soil texture classification from ISIMIP3a protocol soil input data (Volkholz and Müller, 2020). (v) Annual atmospheric CO<sub>2</sub> data from the ISIMIP3a (Büchner and Reyer, 2022). (vi) Six types of daily meteorological for model inputs ( $P_s$ ,  $P_{rc}$ ,  $R_s$ ,  $S_h$ ,  $T_{max}$ ,  $T_{min}$ ,  $T_a$ , U) from the GSWP3-W5E5 dataset for the ISIMIP3a dataset (Lange et al., 2022). We set the data from (i), (ii), and (iv) as constants across the simulation period, whereas the data from (iii), (v), and (vi) are variables.

#### **Analysis**

MATCRO-Maize was first assessed for the phenological simulation of harvest time against the phenological dataset GGCMI (Jägermeyr et al., 2021) and global datasets of crop phenological events for agricultural and earth system modeling which were derived from various field experiments and a phenology model (GCPE; Mori et al., 2023). These datasets were compared under both rainfed and irrigated conditions at a  $0.5^{\circ} \times 0.5^{\circ}$  resolution to check the model's performance. Then, we assessed the yields by combining simulated yield at irrigated and rainfed according to the maize area in each grid cell.

The simulated final yields in each grid cell under irrigated and rainfed conditions were aggregated by grid cell, country and global level with the harvested area from MIRCA2000 data (Portmann et al., 2010) via the following equation for each year from 1981-2010:

$$Yield_{aggregated} = \frac{\sum_{i=1}^{n} (Yield_{i,rf} \times Area_{i,rf}) + \sum_{i=1}^{n} (Yield_{i,irr} \times Area_{i,irr})}{\sum_{i=1}^{n} (Area_{i,rf} + Area_{i,irr})}$$
(39)

where  $Yield_{aggregated}$  is the aggregated yield with the total grid cells (n) in grid cell i.  $Yield_{rf}$  and  $Yield_{irr}$  are the simulated yields under rainfed and irrigated conditions, respectively, and  $Area_{rf}$  and  $Area_{irr}$  are the harvested areas from MIRCA2000 for rainfed and irrigated conditions, respectively.

The model performance was evaluated by comparing its output with the historical yield dataset. The grid cell-level yield was averaged across a 30-year period and compared with the Global Dataset of Historical Yields (GDHY) (Iizumi and Sakai,

2020), 29-year period of GlobalCropYield (GCY, Cao et al., 2025), and year 2010 of Spatial Production Allocation Model (SPAM; IFPRI, 2019). The country and global-level yields were compared with FAOSTAT data (FAOSTAT, 2024) for the average and annual variabilities over the 30 years. In the comparison at the country level, we focus on the top 20 maize-producing countries that account for more than 85% of total maize production.

We focused on two perspectives for evaluation: (i) the ability of the model to capture the spatial distribution of yield in both low and high-producing countries and (ii) the ability of the model to reproduce the climatic effect reflected in the interannual variability at the country and global scales. The first perspective was analysed using NMAE to quantify model error for both the global yield and the yield of the top 20 producing countries. The 30-year average yields were also compared based on the statistics of COR, RMSE, and RRMSE to confirm accuracy. The second perspective was analysed via the COR of the detrended deviation between the simulated and FAOSTAT yields to assess the interannual variability.

## 3 Results

345

350

365

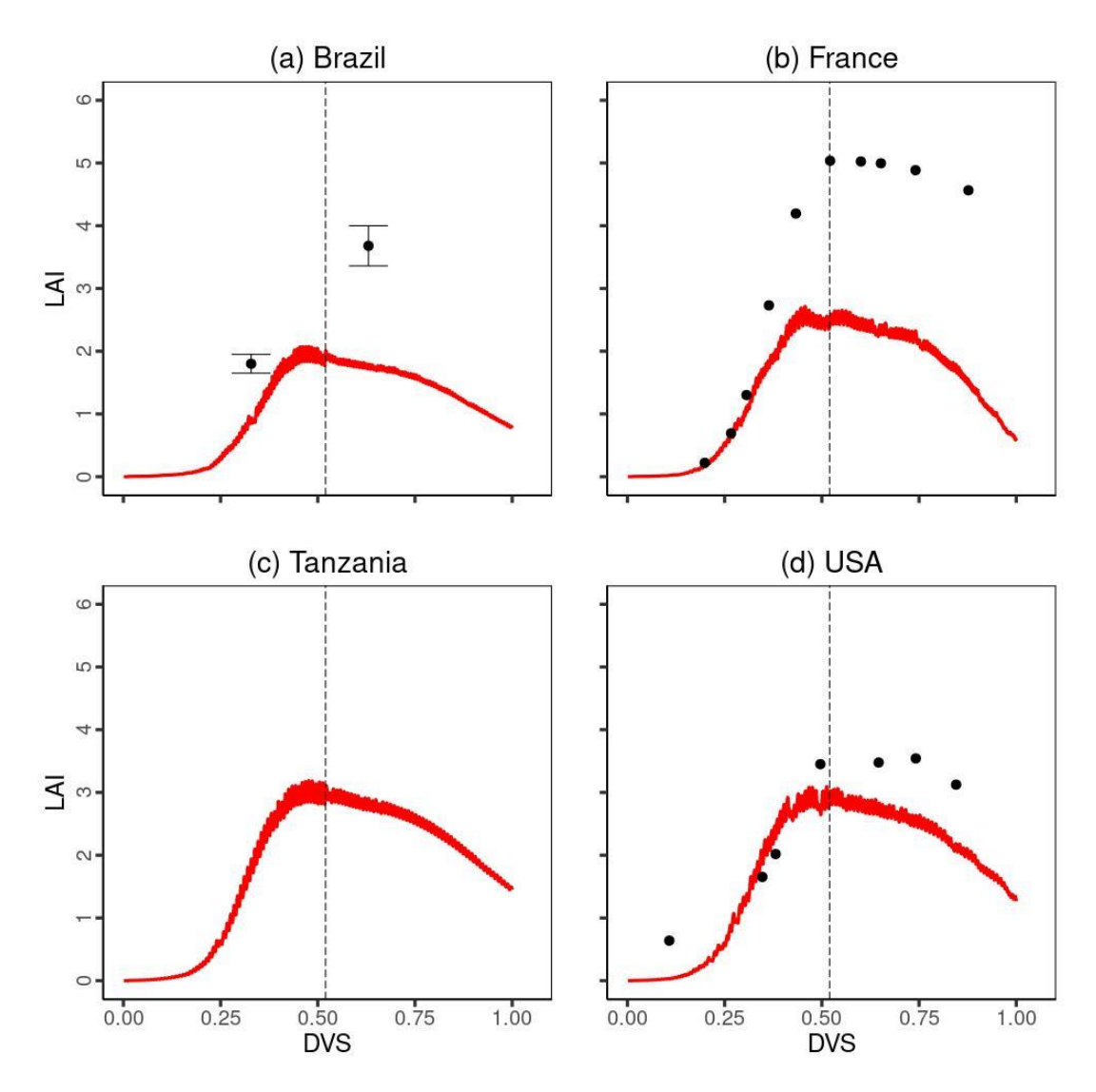
370

# 3.1 Point-scale simulations

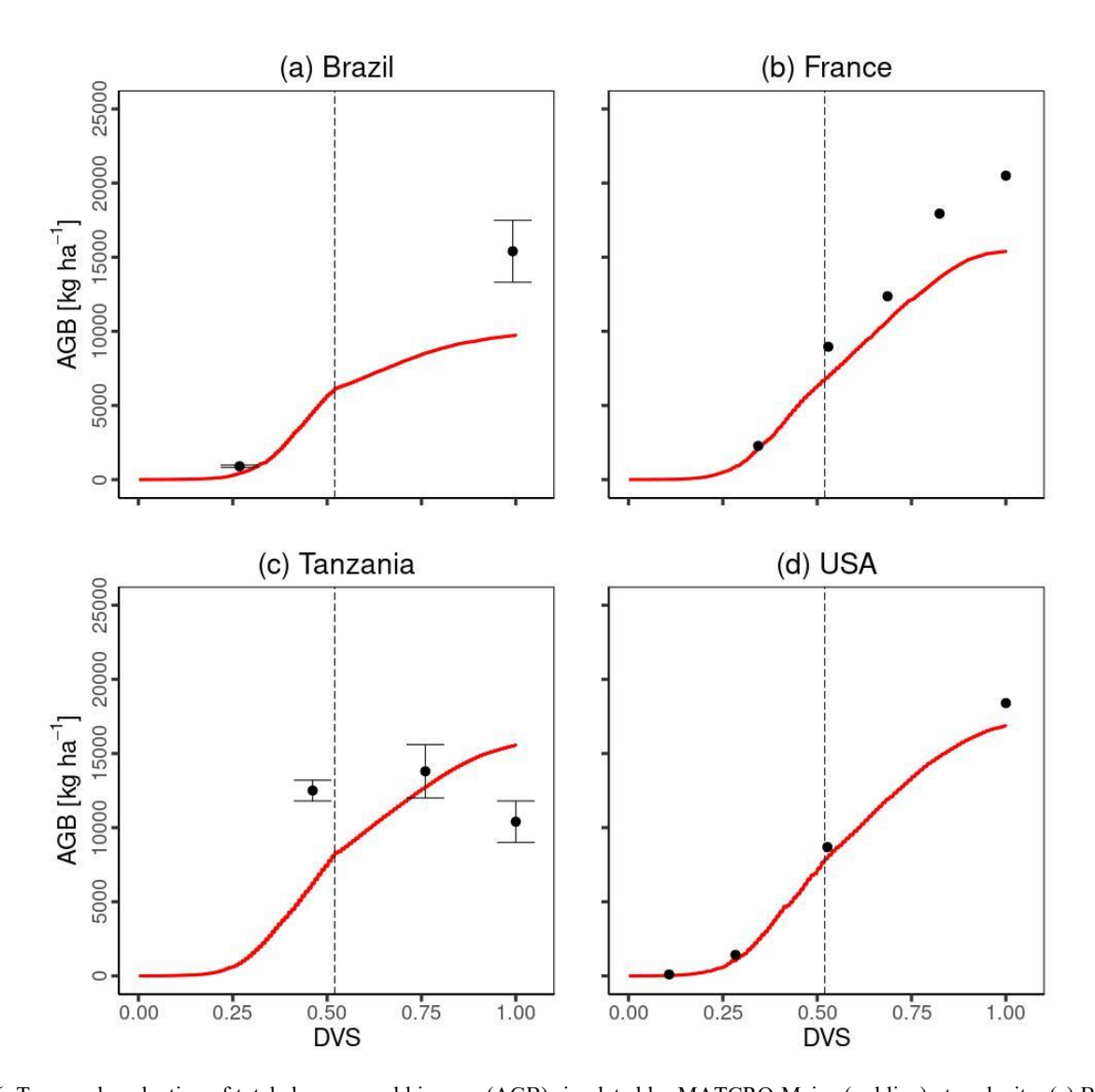
A comparison of the time series changes in the LAI at each experimental site is shown in Figure 5. In general, MATCRO-Maize captured the increasing trend towards flowering time, followed by a decreasing trend towards the end of maturity. Especially during the vegetative stage ( $D_{vs} < D_{vs,flw}$ : 0.52), the simulated LAI showed relatively good agreement. However, the simulated LAI was notably underestimated in Brazil and France immediately before the reproductive stage (near the dashed black line in Fig. 5). The LAI underestimation in France and Brazil (Fig. 5) could also be seen with a large RMSE, which is approximately 50% of the average LAI across all observational values at 3 sites except for Tanzania during the crop growth, although overall, the comparison was statistically significant (p value < 0.01), with a COR of 0.762.

Figure 6 compares the time series of total aboveground biomass between the simulated and experimental data. Except for Tanzania, MATCRO-Maize accurately estimated the increasing trend of total aboveground biomass towards maturity (Figs. 6(a) and 6(b)), although the simulated biomass in Brazil was underestimated at maturity (Fig. 6(a)). The simulated total aboveground biomass in Tanzania increased until maturity, while the observations gradually decreased towards the maturity time (Fig. 6(c)). The comparison of total aboveground biomass during the crop growth was statistically significant (*p* value < 0.001), with a COR of 0.895, although the RMSE was 3,628.3 [kg ha<sup>-1</sup>], which corresponds to approximately 35% of the average of all observed total aboveground biomass.

Figure 7 compares the 1:1 line between the simulated and experimental data for harvested yield. The comparison of the final crop yield was statistically significant (*p* value < 0.01). It had a relatively low COR compared with the LAI and total aboveground biomass, due to the small sample size (N=4) and the overestimation for Tanzania. The RMSE was 2,575.0 [kg ha<sup>-1</sup>], which is approximately 30% of the average observational yield at all the sites. It is noted that Figures 5–7 present the model evaluation using independent data. Evaluation was performed using a global parameter from the literature to simulate the plant organs in the global-scale simulation, which may have resulted in some deviations.



**Figure 5.** Temporal evaluation of leaf area index (LAI) simulated by MATCRO-Maize (red line) at each site: (a) Brazil, (b) France, (c) Tanzania and (d) the USA across the developmental stage ( $D_{vs}$ ). The observation data in each site are shown by black points. Notably, there were no observational data in Tanzania. The error bars were provided only for Brazil. The dashed black line shows the flowering time.



**Figure 6.** Temporal evaluation of total aboveground biomass (AGB) simulated by MATCRO-Maize (red line) at each site: (a) Brazil, (b) France, (c) Tanzania and (d) the USA across the developmental stage ( $D_{vs}$ ). The observation data in each site are shown by black points. The error bars were only provided for Brazil and Tanzania. The dashed black line shows the flowering time.

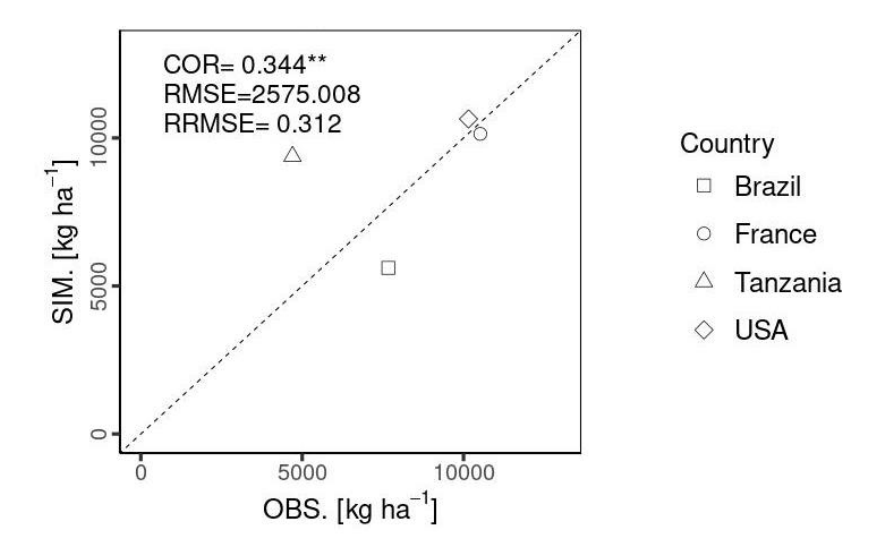


**Figure 7.** Statistical comparison (COR, RMSE, and RRMSE) of maize yield. The x-axis (OBS) represents the observational data, and the y-axis (SIM.) is the simulated data. Shapes show each site: Brazil (square), France (circle), Tanzania (triangle), and the USA (diamond). Notably, there was no observed LAI in Tanzania. The symbols \*\*\*, \*\*, indicate *p* values < 0.001 and 0.01, respectively.

#### 390 3.2 Global-scale simulations

#### 3.2.1 Phenology

395

400

The timing of seasonal biological events (i.e. harvest time) has a significant impact on crop growth and yield outcomes. Global yield is affected by global phenology. We assessed agreement to check the model performance by comparing the difference between simulated global average harvest time (1981–2010) with the gridded global dataset of phenological datasets of GGCMI (Jägermeyr et al., 2021; Figs. 8(a and b)), and GCPE (Mori et al., 2023; Figs. 8(c and d)). The maps show consistent spatial patterns for later harvest time between the simulation and the reference datasets, in parts of Brazil, USA, southern and central Africa. The discrepancies between datasets are likely produced due to the difference in phenology parameterization and management assumptions where GGCMI and GCPE used different methodologies and data sources. Moreover, the use of the average growing degree day in the simulations led to year-to-year differences in harvest time compared with the reference crop calendar used for the input data (Figs. 8(a and b)). The mean absolute differences in harvest time (Figs. 8(e and f)) indicate that the largest biases occur mostly in tropical regions.

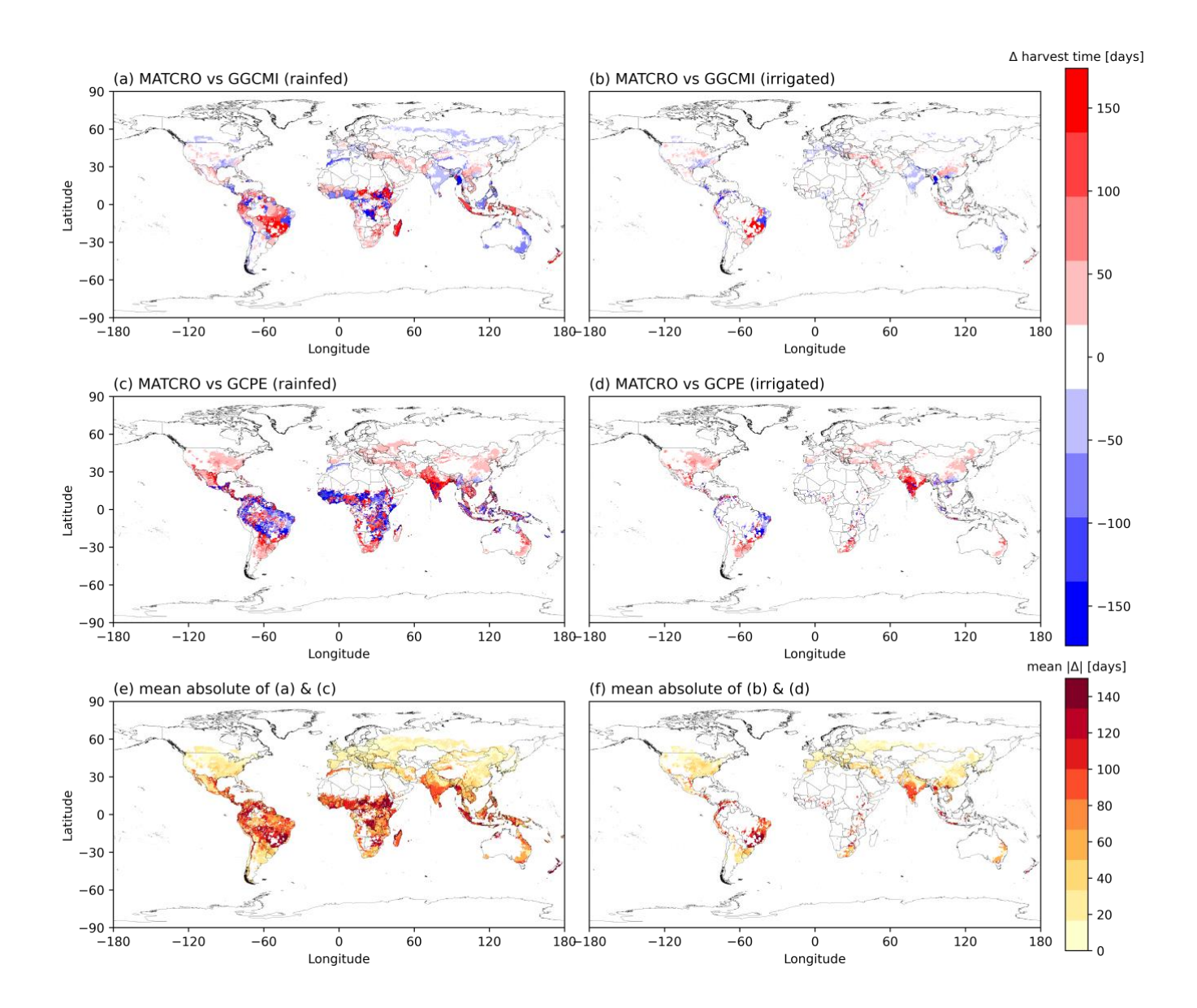
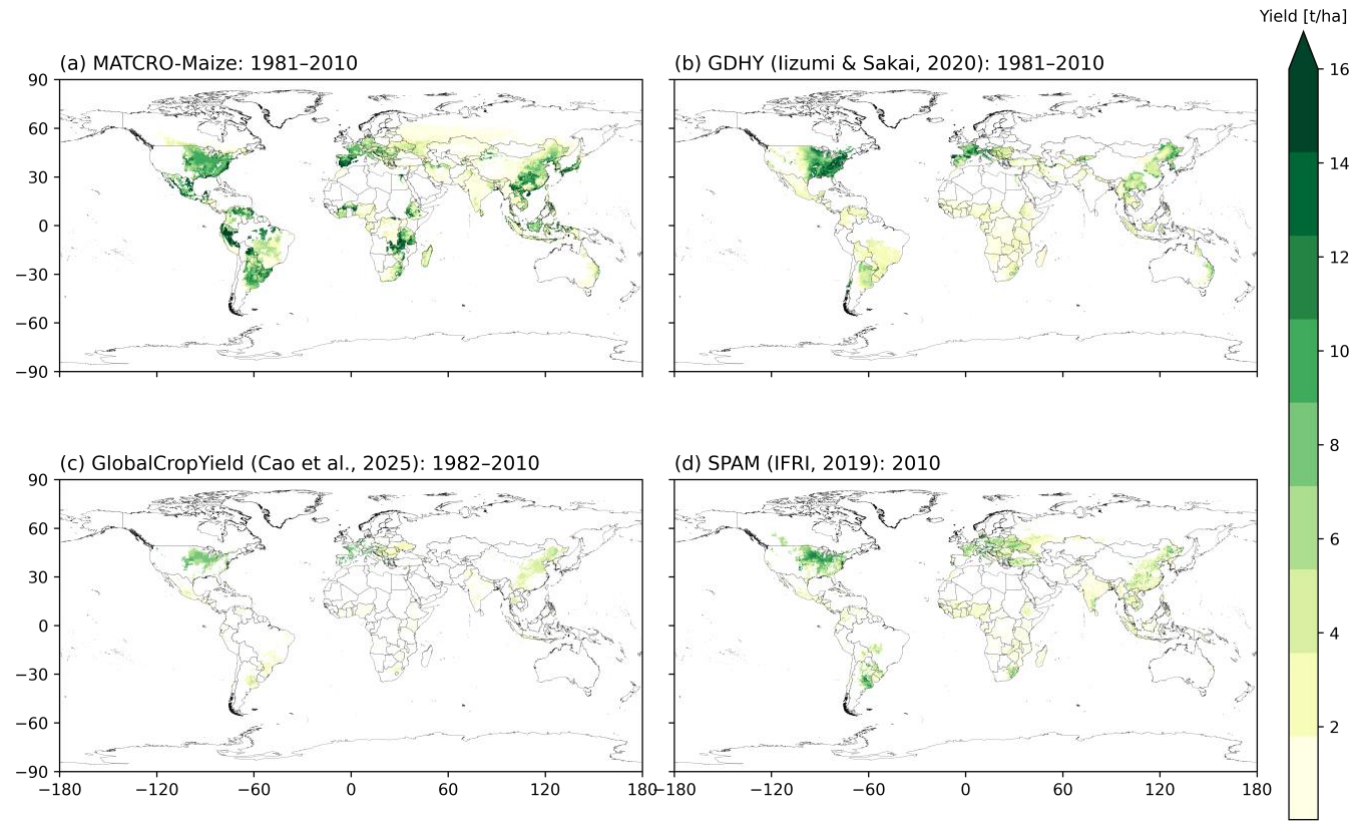


Figure 8. The difference between simulated harvest time (days) in MATCRO-Maize simulations with: (a) GGCMI in the rainfed, and (b) irrigated conditions; (c) GCPE in the irrigated, and (d) rainfed conditions. Blue indicates underestimation, while red indicates overestimation between simulations and references. Panels (e) and (f) show the mean of absolute differences (days) between simulations and two reference datasets under the rainfed (a, c) and irrigated (b, d) conditions, respectively.

# **3.2.2 Yield**

A comparison of the global distributions is shown in Figure 9 (simulations: Fig. 9(a); observation datasets: Figs. 9(b, c, and d)). All datasets were harmonized to a 0.5° × 0.5° resolution, including simulated yield from MATCRO-Maize (Fig. 9(a)), 410 GDHY (lizumi and Sakai, 2020; Fig. 9(b)), GCY (Cao et al., 2025; Fig. 9(c)), and SPAM (IFPRI, 2019; Fig. 9(d)). The data were averaged over 1981–2014 for GDHY, 1982–2014 for GCY, and at the year 2010 for SPAM. While the overestimation is

mainly evident in tropical regions, the simulated yield could capture high-yielding regions, including the Corn Belt in the United States and the northern part of China, in agreement with the reference datasets.



**Figure 9.** Global distribution of the 30-year average (1981-2010) maize yield by (a) simulations from the MATCRO-Maize and (b) the GDHY dataset. For comparison, yield estimates from shorter periods are also shown from (c) GCY for 29-year average (1982-2014) and (d) SPAM2010 for year 2010. The yield is aggregated based on the harvested area from MIRCA2000.

Temporal changes in the global yield across 30 years indicated that although the global yield had an NMAE of 0.67, indicating a simulation error of 67% with respect to the average FAOSTAT yield, the comparison of the interannual variability between the simulations and observations was statistically significant (p value < 0.01), with a COR of 0.549 (Figure 10). For the top 20 producing countries, MATCRO-Maize also tended to overestimate the annual yield (Figure 11) and the average yield over a 30-year period (Figure 12). The overestimation was particularly pronounced in Egypt, where the simulated yield was approximately four times greater over a 30-year period. In terms of interannual variability, half of the 20 countries were statistically significant, with p values < 0.001 for 6 countries, < 0.01 for 2 countries, and < 0.05 for 2 countries (Fig. 11). The 30-year average comparison was also statistically significant (p value < 0.01), with a COR of 0.58, although the RMSE was 4,007.7 [kg ha<sup>-1</sup>], which is almost the same as the average yield of the top 20 maize-producing countries (Fig. 12).

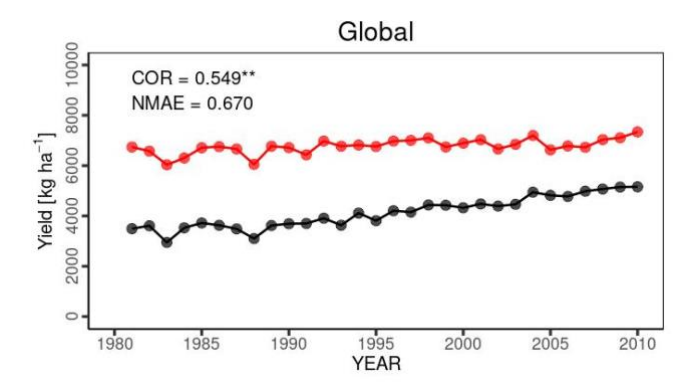


**Figure 10.** Interannual variability in global maize yield from 1981 to 2010 for our simulation (red circles) and FAOSTAT (black) yields. 430 COR represents the correlation coefficient of interannual variability. NMAE means normalized mean absolute error. Asterisks \*\* indicate *p* value < 0.01.

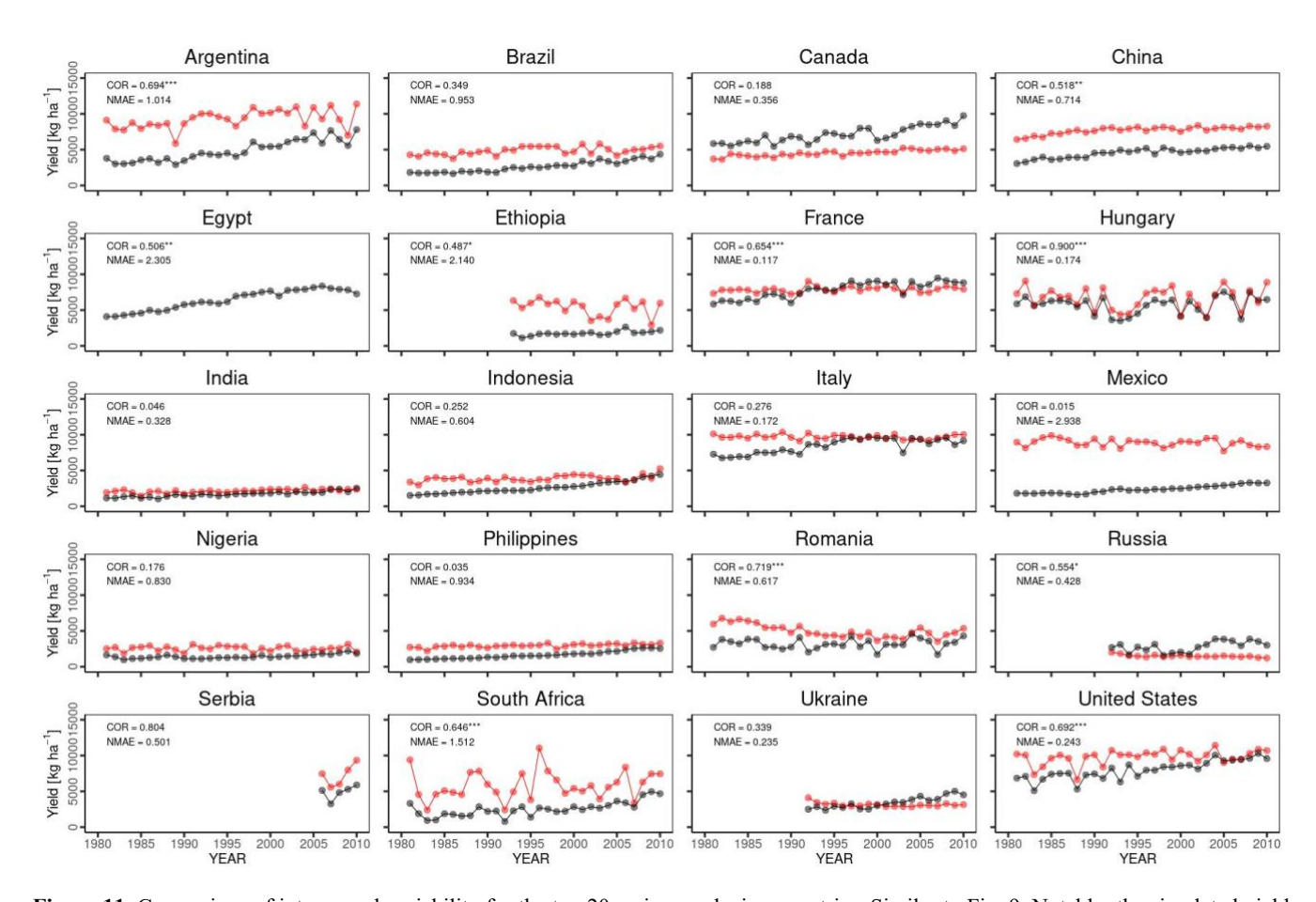


**Figure 11.** Comparison of interannual variability for the top 20 maize-producing countries. Similar to Fig. 9. Notably, the simulated yield in Egypt is not shown as it extends beyond the range of the y-axis. The symbols \*\*\*, \*\*, and \* indicate p values < 0.001, 0.01, and 0.05, respectively.

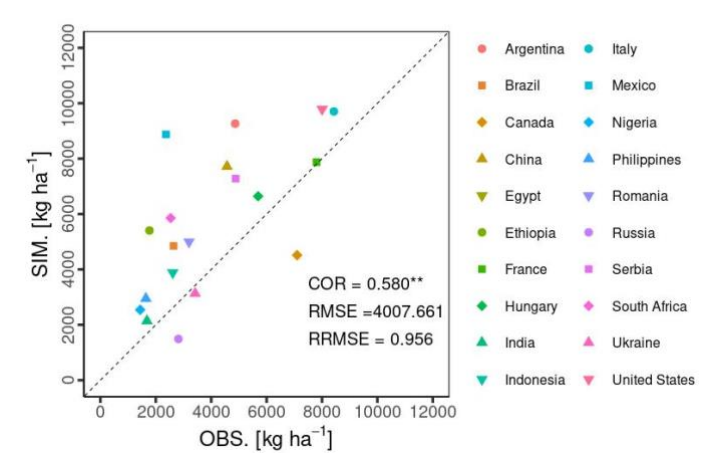


**Figure 12.** Accuracy of the 30-year average of the simulated yield (SIM) to the observed yield (OBS from FAOSTAT data) for the top 20 countries. Symbols show the average yield in each country. Notably, the Egypt data points are not shown as exceeding the range of the y-axis. Asterisks \*\* indicate a *p* value < 0.01.

# 3.3 The effects of photosynthesis and N fertilizer

445

450

In addition to the yield comparison, we analysed the effect of nitrogen fertilizer ( $N_{fert}$ ) on maize yield, as it is a key determinant of crop yield. It compared both simulated yield data and FAOSTAT yield data with  $N_{fert}$  for a 30-year average using a fitted polynomial curve (quadratic polynomial regression). We also conducted two tests to quantify the effects of the  $N_{fert}$ -related function and parameters as follows: (i) Eq. (27) during the vegetative stage is derived from Drouet and Bonhomme (2004), defined as "test  $S_{ln}$ - $V_{cmax}$ ", where  $V_{cmax}$  (0) used this function:

$$V_{cmax}(0) = 36.8 * \left\{ \frac{2}{1 + \exp[-2.45 * (S_{ln} - 0.27)]} - 1 \right\}, D_{vs} < D_{vs,flw}$$
(40)

and (ii)  $S_{ln,plt}$  used parameter value from 0.825 (Table 1) to 0.5 (defined as "test  $S_{ln,plt}$ ").

Figure 13 illustrates the comparison of country-level yield data with nitrogen fertilizer levels: (a) FAOSTAT data, (b) simulated yield by MATCRO-Maize, (c) the impact of reduced Rubisco activity on photosynthetic rates based on experimental data from Drouet and Bonhomme (2004) in the "test Sln-Vcmax" scenario, and (d) the effect of reduced photosynthetic rates due to lower initial specific leaf nitrogen at planting time in the "test Sln,plt" scenario. The nitrogen fertilizer values were derived from gridded dataset of ISIMIP (Volkholz and Ostberg, 2022).

Figures 13 (a) and (b) show the comparisons based on  $N_{fert}$  for each FAOSTAT and simulated yield, respectively.

455 MATCRO has a strong  $N_{fert}$  effect on the yield reflected in the steep upward trend of the fitted curves. This effect was scarcely alleviated by the intentionally reduced effect of photosynthesis (Figs. 13(c and d)), mainly because of the effect of Egypt as an outlier with higher values. Without Egypt as an outlier, the curves for FAOSTAT and MATCRO-Maize were more comparable. The maize yield in Egypt shows high value compared to other countries where significant overestimation was observed.

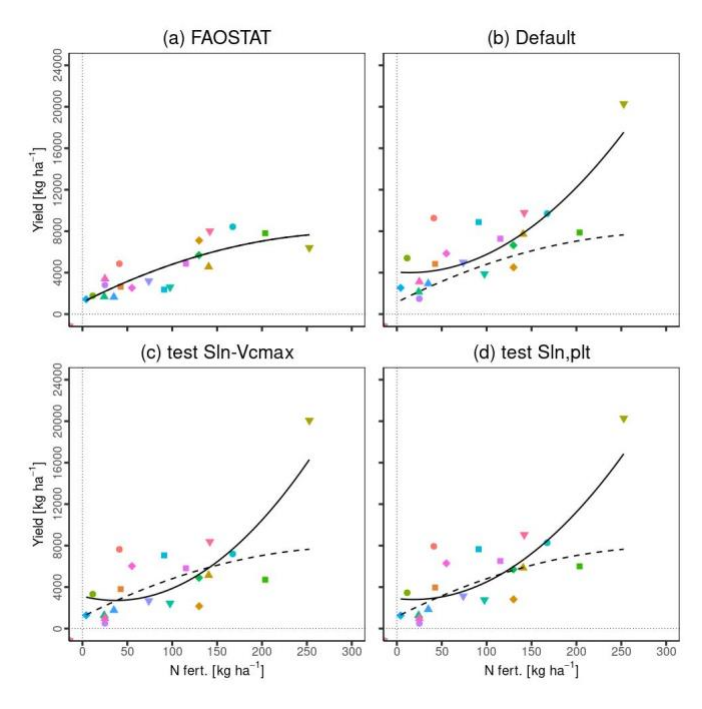


Figure 13. Relationship between  $N_{fert}$  and yield in (a) FAOSTAT data, (b) simulated yield with the original setting (Default), (c) simulated yield with the changed  $S_{ln}$ - $V_{cmax}$  relationship (test Sln-Vcmax), (d) simulated yield with the changed parameter related to the  $D_{vs}$ - $S_{ln}$  function (test Sln, plt).  $N_{fert}$  (N fertilizer) and country yield were averaged across 30 years for each country. The legends for symbols are the same as those in Fig. 11. The solid lines are the fitted curves for the data, while the dashed line in (b), (c), and (d) indicates a fitted curve in (a). All lines were fitted using a quadratic polynomial regression.

## 4 Discussion

460

465

470

#### 4.1 Point-scale simulations

The point-scale simulations were evaluated using global parameters to assess their ability to capture broad yield patterns across different regions. The simulated harvested yield showed statistically significant correlations at the point scale (Fig. 7), indicating that the MATCRO-Maize model could simulate maize growth and yield. However, there were some discrepancies between the simulations and observations that remain due to the limitations of using global parameters, such as the underestimation of the LAI in Brazil and France, the underestimation of the total aboveground biomass in Brazil, and the different growth trends of the total aboveground biomass in Tanzania. The underestimation of LAI is primarily due to the use of global morphological parameters at the site scale. Further investigation will improve site-specific performance by coupling LAI to key soil properties (soil organic carbon, total nitrogen, and water-holding capacity) and by incorporating canopy cover fraction following Hasegawa et al. (2008). Global parameters at the point scale enable testing the model's applicability across various regions, although local variations in soil, climate, or crop management may not be fully captured in this study.

One potential factor contributing to the underestimation of the LAI in France might be related to the effect of plant density, which is not currently considered in MATCRO. The actual plant density [plants m<sup>-2</sup>] at each site was 9.5 (France), 7.5 (USA),

480 6.6 (Brazil), and 9.5 (Tanzania) (Bassu et al., 2014). Some studies have shown that LAI trends are affected primarily by the plant density factor relative to N<sub>fert</sub> and hybrids (Boomsma et al., 2009; Ciampitti et al., 2013a; Ciampitti and Vyn, 2011). MATCRO could not reproduce the trends driven by plant density leading to underestimation, although other important factors (e.g., management practices, climatic conditions), which are quite different from each site in the literature, would also affect crop growth variables, including the LAI.

Both the underestimation of the LAI and total aboveground biomass in Brazil were caused by the field experimental conditions of  $N_{fert} = 0$ , given its effect on crop growth in MATCRO. The reason for the lack of fertilization in the field experiment was that sufficient N was released by organic matter mineralization (Bassu et al., 2014), which was not considered in the model. Moreover,  $N_{fert}$  directly affects  $S_{ln}$  in MATCRO, with an increasing trend towards flowering and then a decreasing trend towards maturity (Fig. 1).  $S_{ln}$  is related to  $V_{cmax25}(0)$ , which in turn affects the photosynthesis calculation (Section 2.1 and Section 2.2.2). In particular, during the reproductive stage, we used Eq. (27), which results in a low  $V_{cmax25}(0)$  under low  $S_{ln}$  due to the more gradual slope of the curve compared with the vegetative stage (1.41 for the reproductive stage, and 2.9 for the vegetative stage, in Eq. (27)), indirectly leading to low biomass accumulation through photosynthesis. This could be attributed to the underestimation of total aboveground biomass at maturity (Fig. 6 (a)). For underestimation of the LAI, low leaf biomass accumulation, which is derived from the same mechanism, would be the reason considering the calculation process of the LAI in MATCRO. The LAI is determined by the division of the leaf biomass weight by  $S_{lw}$ , which depends on  $D_{vs}$ . Because  $S_{lw}$  is calculated from the same parameter at all sites (Eq. (33) and Fig. 3), leaf weight is the factor that causes differences between sites, leading to the underestimation of the LAI in Brazil. Therefore, the condition of  $N_{fert} = 0$  might be the reason for both underestimations.

Another reason for the difference in the growth trend of biomass in Tanzania was related to the length of the growing season. The cultivar used in Tanzania was a short-season type with 99 days of observed growing season length, whereas the cultivars at other sites were medium- or long-season types with lengths ranging from 122 to 173 days (Bassu et al., 2014). Capristo et al. (2007) reported that, compared with medium- and long-season cultivars, short-season cultivars presented the lowest biomass accumulation from flowering to maturity, which was reflected in the observed biomass (Fig. 6 (c)). This suggests that the trend of biomass accumulation varies across growing season types. Although other factors, such as climatic conditions or biotic stresses, could also affect the biomass accumulation. While MATCRO considers the growing season length as  $G_{ad,m}$  to judge the harvesting time, this does not mean that MATCRO could capture the difference in trends due to growing season types, leading to the gap between the simulations and observations shown in Tanzania.

## 4.2 Global-scale simulations

485

490

495

500

A comparison of the global distribution of maize yield revealed that MATCRO-Maize could capture the distribution of high-510 yield regions but could not capture the yield in tropical regions (Figures 8 and 9). Similar overestimations in tropical regions have also been reported in other global models, possibly because of the lack of representation of extreme weather events or crop pests (Lombardozzi et al., 2020; Osborne et al., 2015). Moreover, soil fertility is also an important source of model error and contributes to spatial variation.

Notably, MATCRO-Maize tended to overestimate the absolute values for global yield and the yields of the top 20 countries, as reflected in the NMAE and RMSE values (Figures 10, 11, and 12). The simulated total global yield is mainly determined by the yields of the top three maize-producing countries: the United States, China, and Brazil, which have large cultivation areas (Table 3). The yields of all three countries were overestimated, with simulated yields approximately 1.2, 1.7, and 1.8 times greater than the 30-year averages in the United States, China, and Brazil, respectively, leading to an overestimation of the total global yield. Such overestimations in the main producing countries, especially in China and Brazil, are also observed in other global crop models (Von Bloh et al., 2018; Osborne et al., 2015; Schaphoff et al., 2018). This indicates that there are factors important for determining yields that are not considered in most crop models.

515

520

525

530

535

540

545

For the top 20 producing countries, the overestimation was particularly strong in Egypt, with a simulated yield approximately four times greater than that reported by FAOSTAT. This overestimation is caused by the irrigated conditions in all grids in Egypt. Under simulation in rainfed conditions, crop growth in Egypt was not simulated in the model due to the inhibited photosynthesis rate caused by strong water stress. Under irrigated conditions, this strong water stress was alleviated. In addition, the radiation in Egypt was consistently strong throughout the growing period, and  $N_{fert}$  was highest among the top 20 countries across the 30 years simulated, increasing from approximately 180 kg ha<sup>-1</sup> in 1980 to 360 kg ha<sup>-1</sup> in 2010. This caused the photosynthesis rate to be high (Eq. (4)) across the growing seasons, leading to marked overestimation.

The current version of MATCRO-Maize can reproduce yield responses to nitrogen fertilization across a range of fertilizer levels, but it tends to overestimate yields under certain conditions (e.g., Egypt). This occurs because the model assumes high nitrogen use efficiency and idealized irrigation conditions, where actual yields are constrained by soil quality, management, and local cultivar traits not explicitly represented. This suggests that the representation of nitrogen effects in the model remains simplified, and further refinement is needed for region-specific scale simulation.

Although the simulated yield has the large error in terms of the absolute value, the comparison of the 30-year average yield was statistically significant, with a COR of 0.58 (*p* value < 0.01) and an RMSE of 4,008 kg ha<sup>-1</sup> (Fig. 12), showing the ability to capture the spatial distribution of the yield both in low- and high-producing countries from the first perspective of the comparison (Section 2.3.2). This result was comparable to another model, LPJ-GUESS (Olin et al., 2015), with a COR of 0.46 and an RMSE of 4,300 kg ha<sup>-1</sup> (Table 4). Although the targeted countries differed (top 20 producing countries for MATCRO-Maize, and whole countries for LPJ-GUESS).

In terms of interannual variability from the second perspective, the total global yield and approximately one-third of the top 20 producing countries were statistically significant, with p values < 0.01 (Figs. 10 and 11). It indicates that MATCRO-Maize could reproduce the climatic effect globally to some extent. This result is also supported by similar comparisons of other global crop models in terms of statistics (Table 4). However, it is difficult to simply compare the statistical values between the models owing to the differences in periods, input data, and methods for detrending and aggregating the yield. The COR of interannual variability for total global yield in MATCRO-Maize was in the range of those of the other models (0.55; 0.42 $\sim$ 0.89,

respectively). For the top 20 countries, almost all the COR values also fell within the range of the other models. Therefore, these comparisons from two perspectives might indicate that MATCRO-Maize reproduces reasonable results. The moderate correlations observed reflect the typical influence of yield data variability and uncertainty in management practices across regions.

Table 3. Maize cultivated land area for 20 major producer countries from MIRCA2000 (Portmann et al., 2010).

Country	Total area [ha]	Rainfed area [ha]	Irrigated area [ha]
Argentina	3,248,715.9	3,147,580.7	101,135.3
Brazil	11,223,262.5	11,120,154.9	103,107.6
Canada	1,364,585.3	1,328,206.2	36,379.1
China	24,376,805.2	11,615,190.0	12,761,615.2
Egypt	827,766.1	0.0	827,766.1
Ethiopia	1,172,231.1	1,084,795.6	87,435.5
France	3,128,401.0	2,257,380.0	871,021.0
Hungary	1,057,610.7	1,052,622.6	4,988.1
India	6,294,770.9	4,833,685.9	1,461,085.0
Indonesia	3,479,825.7	3,135,443.9	344,381.8
Italy	1,322,692.9	534,281.4	788,411.5
Mexico	7,459,039.5	5,852,617.4	1,606,422.1
Nigeria	3,686,757.3	3,667,564.5	19,192.8
Philippines	2,590,081.0	2,590,081.0	0.0
Romania	3,139,981.1	3,016,990.5	122,990.6
Russia	4,206,747.0	3,594,403.2	612,343.9
Serbia	1,074,614.2	1,062,985.8	11,628.4
South Africa	3,060,053.5	2,930,208.2	129,845.4
Ukraine	3,382,783.5	3,194,146.2	188,637.3
United States	31,307,667.3	26,508,600.7	4,799,066.7

			C	OR of inte	erannual v	ariability		
References	Period	Global	USA	China	Brazil	Mexic	France	Argenti
						o		na
MATCRO-	1981-	0.549**	0.692***	0.518*	0.349	0.015	0.654***	0.694***
Maize	2010	0.349	0.092	*				
JULES-crop <sup>1a</sup>	1961-	0.48	0.43	0.12	0.12	0.061	0.52	0.57
	2008	0.40	0.43	0.12				
LPJmL4 <sup>2b</sup>	1981-		0.675***	$0.676^{*}$	0.169	-0.124	-0.331	0.717***
	2010	_	0.073	**				
LPJmL5 <sup>3c</sup>	1981-		0.686***	0.641*	0.059	0.0618	$0.461^{*}$	0.650***
	2010	_	0.080	**	** 1			
GGCMI phase	1981-	_	0.817	0.245	0.029	_	0.649	0.727
3 <sup>4d</sup>	2015							
GGCMI phase	1982-	$0.42^{**} \sim 0.8$	0.89	0.75	0.66	0.85	0.87	0.85
1 <sup>5e</sup>	2006	9***						
			C	OR of inte	rannual v	ariability		
References	Period	Romania	South	India	Italy	Hunga	Indonesi	Ukraine
			Africa			ry	a	
MATCRO-	1981-	0.719***	0.646***	0.046	0.276	$0.900^{*}$	0.252	0.339
Maize	2010					**		
JULES-crop <sup>1a</sup>	1961-	0.32	0.41	0.34	0.34	0.33	0.065	_
	2008							
LPJmL4 <sup>2b</sup>	1981-	_	0.711***	-0.22	-	_	0.124	-0.046
	2010							
LPJmL5 <sup>3c</sup>	1981-	_	0.667***	$0.496^{*}$	-	_	-0.163	0.152
	2010			*				
GGCMI phase	1981-	_	_	-	-	-	_	_
$3^{4d}$	2015							
GGCMI phase	1982-	0.90	0.91	0.76	0.76	0.90	0.42	0.61
1 <sup>5e</sup>	2006							
		30-year	averaged yield					
References	Period	COR	RMSE [kg					
			ha <sup>-1</sup> ]					

MATCRO-	1981-	0.580**	4,008
Maize	2010		
LPJ-GUESS <sup>6f</sup>	1996-	0.46	4,300
	2005		

<sup>&</sup>lt;sup>1</sup> Countries-level comparison was conducted for 12 countries, which were detrended only for observation. p values are not shown.

580 5 Fourteen global gridded crop models were used. The COR of the global yield shown here is the minimum and maximum value, except for one nonsignificant correlation with the default setting. The COR of each country shown here is the best correlation among the 14 models, including 3 different settings with statistical significance (p values are not shown). For both the global and country-level comparisons, a 5-year moving average was used to remove trends.

- 585 a Osborne et al., 2015
  - <sup>b</sup> Schaphoff et al., 2018
  - <sup>c</sup> Bloh et al., 2018
  - d Jägermeyr et al., 2021
  - e Müller et al., 2017
- 590 f Olin et al., 2015

<sup>&</sup>lt;sup>2,3</sup> Countries-level comparison was conducted for the top 10 producing countries, which were detrended via a 5-year moving average.

<sup>&</sup>lt;sup>4</sup> Twelve global gridded crop models were used. The COR shown here is the ensembled mean value for the 5 largest producing countries after detrending. *p* values are not shown.

<sup>&</sup>lt;sup>6</sup> The 10-year average comparisons included all countries. *p* values are not shown.

## 4.3 Model limitations

595

600

605

610

615

620

MATCRO-Maize currently lacks explicit simulation of soil organic carbon and soil nitrogen mineralization. Instead, the effects of nitrogen supply are represented by describing the relationship between a broad range of nitrogen fertilization levels (Muchow, 1988) and specific leaf nitrogen (SLN), which subsequently affects photosynthetic capacity (Vcmax). While this simplification allows for global-scale application, it limits the model's ability to accurately represent nitrogen balance in maize yield at specific sites. Yield variations can be influenced by soil organic carbon and nitrogen, which are affected by farming practices and contribute to soil fertility (Ma et al., 2023). Future development could involve coupling MATCRO with a mechanistic soil nitrogen and carbon module to a dynamic plant nitrogen balance. This would enhance the model ability to capture nitrogen dynamics under varying soil types and management practices.

The strong  $N_{fert}$  effect shown in the evaluation (underestionation found in Brazil for the point scale comparison) and comparison based on the  $N_{fert}$  and yield (Figure 13). In the model,  $N_{fert}$  has a direct relationship with  $S_{ln}$  (Eq. (28)) and consequently affects  $V_{cmax25}$  (0) through the function  $S_{ln}$ - $V_{cmax25}$  (0) (Eq. (27)). Therefore, the strong  $N_{fert}$  effect is caused by either the former, the latter, or both processes. Few studies have explicitly shown time series changes in  $S_{ln}$  and  $S_{ln}$ - $V_{cmax}$  relationships from experiments. We used some of them to establish the functions shown in Eqs. (27) and (28) (Section 2.2.2) at this stage, resulting in a strong  $N_{fert}$  effect in the model. However, the intentional experiment indicated that the changed relationships could partly reproduce the adequate effect, which was observed in the FAOSTAT yield. This might mean that the established functions include a degree of uncertainty. Nitrogen effects are represented indirectly via SLN as a function of fertilizer rate and developmental stage, which constrains the model ability to capture nitrogen cycling in soils and plants. Incorporating broader experimental data could refine the model's nitrogen response and improve maize yield simulations.

In this study, we applied global parameters to simulate the global yield across all grid cells and throughout the years without considering cultivar differences. As mentioned in Section 3.1.2, the trend of biomass accumulation would differ across growing season types. A limitation of the current study is the use of global parameters at the site scale leads to discrepancies between site-level and country-level simulations. Although MATCRO-Maize shows relatively weak correlations at the site scale due to the use of generalized parameters that do not account for local varieties and management, the model demonstrates consistent and statistically significant performance at country and global levels. This indicates that MATCRO-Maize is well suited for capturing large-scale yield patterns and for application in global gridded crop modeling, while recognizing its limited capacity for precise site-specific prediction. However, global-scale simulation results tend to overestimate yield due to LAI being directly driven by carbon balance, which can create feedback that produce excessively high LAI. Future improvements should incorporate constraints on LAI expansion and adjust leaf partitioning when LAI exceeds realistic levels.

Moreover, in major producing countries, such as the United States and China, some studies have shown that there is genetic gain in terms of maize yield (Cooper et al., 2014; Duvick et al., 2003; Liu et al., 2021). Such cultivar differences and long-term genetic improvements are not included in the current MATCRO-Maize. This finding indicates that the generic parameterization used in the model are simple in accounting for the diversity of crop cultivars (Lombardozzi et al., 2020),

partly leading to a gap between the simulations and observations, which is recognized as a limitation of the global model (Osborne et al., 2015). Other important factors that are not considered in the current MATCRO include biotic stresses (e.g., diseases, pests) and detailed management practices (e.g., plant density, as mentioned in Section 4.1) as it affects crop growth and final yield. Further improvement to incorporate such factors with reliable  $N_{fert}$ -related functions could be needed to contribute to more accurate simulations and contribute to studies on the interaction between climate and agriculture.

## **5** Conclusions

We developed a process-based crop model for maize yield estimation, called MATCRO-Maize, by incorporating C4 leaf-level photosynthesis and some crop-specific parameters into MATCRO. The model was first evaluated at the point scale, showing a somewhat reasonable accuracy considered with the available field-based information for parameterization. The calibrated parameters were set from point-scale experimental data and used uniformly in the global-scale simulation. MATCRO-Maize could represent the spatial distribution well and showed reasonable responses to climatic variability, where the results were comparable with those of other studies in terms of statistics. The strong nitrogen fertilizer effect was one of the MATCRO limitations, while the established functions related to nitrogen fertilizer in the model have a degree of uncertainty. Further experimental data under more comprehensive conditions might improve the model. Overall, MATCRO-Maize could contribute to climate effect studies through its ability to be integrated with the LSM for crop growth and the interactions between climate and agriculture.

640 Code and data availability.

The source code used in this study is archived at https://doi.org/10.5281/zenodo.14869445 (Nagata et al., 2025).

Author contributions.

TK supervised this study and acquired the funding. YM developed the model source code and supervised this study. MN adjusted the source code for this study, performed the model simulations, and analysed the model output. MN prepared the original draft, which was reviewed by TK, YM, and AY. The final manuscript was written by MN and revised by AY during the academic publishing process, then approved by all the authors.

Acknowledgements.

645

650

This research was funded by JSPS KAKENHI grant number JP 22k18497. This study was partly supported by the Environment Research and Technology Development Fund (JPMEERF20202005) of the Environmental Restoration and Conservation Agency (ERCA) and JSPS KAKENHI Grant Number JP23H00351.

We thank all the contributors. Dr. Jean-Louis Durand at the French National Research Institute for Agriculture, Food, and Environment (INRAE) provided the observational data at the four sites, which we used to evaluate our model at the point scale.

## References

- Allen R.G., Pereira L.S., Raes D., and Smith M.: Crop Evapotranspiration: Guidelines for Computing Crop Water Requirements FAO Irrigation and drainage paper 56, FAO Food and Agriculture Organization of the United Nations, Rome, 1998.
  - Asseng, S., Ewert, F., Rosenzweig, C., Jones, J. W., Hatfield, J. L., Ruane, A. C., Boote, K. J., Thorburn, P. J., Rötter, R. P., Cammarano, D., Brisson, N., Basso, B., Martre, P., Aggarwal, P. K., Angulo, C., Bertuzzi, P., Biernath, C., Challinor, A.
- J., Doltra, J., Gayler, S., Goldberg, R., Grant, R., Heng, L., Hooker, J., Hunt, L. A., Ingwersen, J., Izaurralde, R. C., Kersebaum, K. C., Müller, C., Naresh Kumar, S., Nendel, C., O'Leary, G., Olesen, J. E., Osborne, T. M., Palosuo, T., Priesack, E., Ripoche, D., Semenov, M. A., Shcherbak, I., Steduto, P., Stöckle, C., Stratonovitch, P., Streck, T., Supit, I., Tao, F., Travasso, M., Waha, K., Wallach, D., White, J. W., Williams, J. R., and Wolf, J.: Uncertainty in simulating wheat yields under climate change, Nat Clim Chang, 3, 827–832, https://doi.org/10.1038/NCLIMATE1916, 2013.
- 665 Ball J.T: An analysis of Stomatal Conductance, Stanford University, CA, USA, 1988.
  - Bassu, S., Brisson, N., Durand, J. L., Boote, K., Lizaso, J., Jones, J. W., Rosenzweig, C., Ruane, A. C., Adam, M., Baron, C.,
    Basso, B., Biernath, C., Boogaard, H., Conijn, S., Corbeels, M., Deryng, D., De Sanctis, G., Gayler, S., Grassini, P.,
    Hatfield, J., Hoek, S., Izaurralde, C., Jongschaap, R., Kemanian, A. R., Kersebaum, K. C., Kim, S. H., Kumar, N. S.,
    Makowski, D., Müller, C., Nendel, C., Priesack, E., Pravia, M. V., Sau, F., Shcherbak, I., Tao, F., Teixeira, E., Timlin, D.,
- and Waha, K.: How do various maize crop models vary in their responses to climate change factors?, Glob Chang Biol, 20, 2301–2320, https://doi.org/10.1111/gcb.12520, 2014.
  - von Bloh, W., Schaphoff, S., Müller, C., Rolinski, S., Waha, K., and Zaehle, S.: Implementing the nitrogen cycle into the dynamic global vegetation, hydrology, and crop growth model LPJmL (version 5.0), Geosci Model Dev, 11, 2789–2812, https://doi.org/10.5194/gmd-11-2789-2018, 2018.
- Bonan, G. B., Lawrence, P. J., Oleson, K. W., Levis, S., Jung, M., Reichstein, M., Lawrence, D. M., and Swenson, S. C.: Improving canopy processes in the Community Land Model version 4 (CLM4) using global flux fields empirically inferred from FLUXNET data, J Geophys Res, 116, 1–22, https://doi.org/10.1029/2010JG001593, 2011.
- Bondeau, A., Smith, P. C., Zaehle, S., Schaphoff, S., Lucht, W., Cramer, W., Gerten, D., Lotze-campen, H., Müller, C., Reichstein, M., and Smith, B.: Modelling the role of agriculture for the 20th century global terrestrial carbon balance, Glob
  Chang Biol, 13, 679–706, https://doi.org/10.1111/J.1365-2486.2006.01305.X, 2007.

- Boomsma, C. R., Santini, J. B., Tollenaar, M., and Vyn, T. J.: Maize morphophysiological responses to intense crowding and low nitrogen availability: an analysis and review, Agron J, 101, 1426–1452, https://doi.org/10.2134/AGRONJ2009.0082, 2009.
- Bouman, B. A. M., Kropff, M., Tuong, T., Wopereis, M., ten Berge, H., and van Laar, H.: Oryza2000: modeling lowland rice,

  International Rice Research Institute, and Wageningen: Wageningen University and Research Centre, Philippines and
  Wageningen, the Netherlands, 235 pp., 2001.
  - Büchner, M. and Reyer, P. O., C.: ISIMIP3a atmospheric composition input data (v1.2). ISIMIP Repository., https://doi.org/https://doi.org/10.48364/ISIMIP.664235.2, 2022.
- Campbell, G. S. and Norman, J. M.: An Introduction to Environmental Biophysics, Springer New York, NY, New York, USA, https://doi.org/10.1007/978-1-4612-1626-1, 1998.
  - Cao, J., Zhao Z., Xiangzhong L., Yuchuan L., Jialu X., Jun X., Jichong H., and Fulu T. Mapping global yields of four major crops at 5-minute resolution from 1982 to 2015 using multi-source data and machine learning. Scientific Data 12, 1, 357, 2025.
- Capristo, P. R., Rizzalli, R. H., and Andrade, F. H.: Ecophysiological yield components of maize hybrids with contrasting maturity, Agronomy Jornal, 99, 1111–1118, https://doi.org/10.2134/agronj2006.0360, 2007.
  - Ciampitti, I. A. and Vyn, T. J.: A comprehensive study of plant density consequences on nitrogen uptake dynamics of maize plants from vegetative to reproductive stages, Field Crops Res, 121, 2–18, https://doi.org/10.1016/J.FCR.2010.10.009, 2011.
- Ciampitti, I. A., Murrell, S. T., Camberato, J. J., Tuinstra, M., Xia, Y., Friedemann, P., and Vyn, T. J.: Physiological dynamics of maize nitrogen uptake and partitioning in response to plant density and N stress factors: I. Vegetative phase, Crop Sci, 53, 2105–2119, https://doi.org/10.2135/cropsci2013.01.0040, 2013a.
  - Ciampitti, I. A., Murrell, S. T., Camberato, J. J., Tuinstra, M., Xia, Y., Friedemann, P., and Vyn, T. J.: Physiological dynamics of maize nitrogen uptake and partitioning in response to plant density and nitrogen stress factors: II. reproductive phase, Crop Sci, 53, 2588–2602, https://doi.org/10.2135/cropsci2013.01.0041, 2013b.
- 705 Collatz, G., Ribas-Carbo, M., and Berry, J.: Coupled photosynthesis-stomatal conductance model for leaves of C4 plants, Functional Plant Biology, 19, 519, https://doi.org/10.1071/PP9920519, 1992.
  - Collatz, G. J., Ball, J. T., Grivet, C., and Berry, J. A.: Physiological and environmental regulation of stomatal conductance, photosynthesis and transpiration: a model that includes a laminar boundary layer, Agric For Meteorol, 54, 107–136, https://doi.org/10.1016/0168-1923(91)90002-8, 1991.
- Cooper, M., Gho, C., Leafgren, R., Tang, T., and Messina, C.: Breeding drought-tolerant maize hybrids for the US corn-belt: discovery to product, J Exp Bot, 65, 6191–6204, https://doi.org/10.1093/jxb/eru064, 2014.
  - Dai, Y., Dickinson, R. E., and Wang, Y. P.: A two-big-leaf model for canopy temperature, photosynthesis, and stomatal conductance, J Clim, 17, 2281–2299, https://doi.org/10.1175/1520-0442(2004)017<2281:ATMFCT>2.0.CO;2, 2004.

- Drouet, J. L. and Bonhomme, R.: Effect of 3D nitrogen, dry mass per area and local irradiance on canopy photosynthesis within leaves of contrasted heterogeneous maize crops, Ann Bot, 93, 699–710, https://doi.org/10.1093/aob/mch099, 2004.
  - Duvick, D. N., Smith, J. S. C., and Cooper, M.: Long-term selection in a commercial hybrid maize breeding program, Plant Breeding Reviews, Wiley, 109–151, https://doi.org/10.1002/9780470650288.ch4, 2003.
  - FAO: Agricultural production statistics 2000–2021, FAO, Rome, Italy, https://doi.org/10.4060/cc3751en, 2022.
- FAOSTAT Production / Crops and livestock products Metadata, https://www.fao.org/faostat/en/#data/QCL/metadata (last access: 31 December 2024), 2024.
  - Hajima, T., Watanabe, M., Yamamoto, A., Tatebe, H., Noguchi, M. A., Abe, M., Ohgaito, R., Ito, A., Yamazaki, D., Okajima, H., Ito, A., Takata, K., Ogochi, K., Watanabe, S., and Kawamiya, M.: Development of the MIROC-ES2L Earth system model and the evaluation of biogeochemical processes and feedbacks, Geosci Model Dev, 13, 2197–2244, https://doi.org/10.5194/GMD-13-2197-2020, 2020.
- Hasegawa, T., Sawano, S., Goto, S. et al. A model driven by crop water use and nitrogen supply for simulating changes in the regional yield of rain-fed lowland rice in Northeast Thailand. Paddy Water Environ 6, 73–82, https://doi.org/10.1007/s10333-007-0099-1, 2008.
  - International Food Policy Research Institute (IFPRI), Global Spatially-Disaggregated Crop Production Statistics Data for 2010 Version 2.0, https://doi.org/10.7910/DVN/PRFF8V, Harvard Dataverse, V4, 2019.
- 730 Iizumi, T., Sakai, T. The global dataset of historical yields for major crops 1981-2016. Scientific Data 7, 97, https://doi.org/10.1038/s41597-020-0433-7, 2020.
  - Iizumi, T., Masaki, Y., Takimoto, T., and Masutomi, Y.: Aligning the harvesting year in global gridded crop model simulations with that in census reports is pivotal to national-level model performance evaluations for rice, European Journal of Agronomy, 130, 126367, https://doi.org/10.1016/J.EJA.2021.126367, 2021.
- 735 Intergovernmental Panel on Climate Change (IPCC): Technical Summary, in: Climate Change 2022 Impacts, Adaptation and Vulnerability, Cambridge University Press, 37–118, https://doi.org/10.1017/9781009325844.002, 2023.
  - Jägermeyr, J., Müller, C., Ruane, A. C., Elliott, J., Balkovic, J., Castillo, O., Faye, B., Foster, I., Folberth, C., Franke, J. A.,
    Fuchs, K., Guarin, J. R., Heinke, J., Hoogenboom, G., Iizumi, T., Jain, A. K., Kelly, D., Khabarov, N., Lange, S., Lin, T.
    S., Liu, W., Mialyk, O., Minoli, S., Moyer, E. J., Okada, M., Phillips, M., Porter, C., Rabin, S. S., Scheer, C., Schneider, J.
- M., Schyns, J. F., Skalsky, R., Smerald, A., Stella, T., Stephens, H., Webber, H., Zabel, F., and Rosenzweig, C.: Climate impacts on global agriculture emerge earlier in new generation of climate and crop models, Nat Food, 2, 873–885, https://doi.org/10.1038/s43016-021-00400-y, 2021.
  - Kanai, R. and Edwards, G. E.: The Biochemistry of C 4 Photosynthesis, C4 plant biology, Elsevier, 49–87, 1999.
- Kinose, Y. and Masutomi, Y.: Impact assessment of climate change on rice yield using a crop growth model and activities toward adaptation: targeting three provinces in Indonesia, Adaptation to Climate Change in Agriculture: Research and Practices, Springer, Singapore, 67–80, https://doi.org/10.1007/978-981-13-9235-1 5, 2019.

- Kinose, Y., Masutomi, Y., Shiotsu, F., Hayashi, K., Ogawada, D., Gomez-Garcia, M., Matsumura, A., Takahashi, K., and Fukushi, K.: Impact assessment of climate change on the major rice cultivar ciherang in Indonesia, Journal of Agricultural Meteorology, 76, 19–28, https://doi.org/10.2480/agrmet.D-19-00045, 2020.
- Knapp, A. K. and Medina, E.: Success of C4 photosynthesis in the field; lessons from communities dominated by C4 plants, C4 plant biology, Elsevier, 251–277, 1999.
  - Lange, S., Mengel, M., Treu, S., and Büchner, M.: ISIMIP3a atmospheric climate input data (v1.0). ISIMIP Repository., https://doi.org/10.48364/ISIMIP.982724, 2022.
- Lawrence D., Fisher R., Koven C., Oleson K., Swenson S., and Vertenstein M: Technical Description of Version 5.0 of the Community Land Model (CLM)., NCAR, 2020.
  - Levis, S., Gordon, B. B., Erik Kluzek, Thornton, P. E., Jones, A., Sacks, W. J., and Kucharik, C. J.: Interactive Crop Management in the Community Earth System Model (CESM1): Seasonal influences on land-atmosphere fluxes, J Clim, 25, 4839–4859, https://doi.org/10.1175/JCLI-D-11-00446.1, 2012.
- Lin, T., Song, Y., Lawrence, P., Kheshgi, H. S., and Jain, A. K.: Worldwide maize and soybean yield response to environmental and management factors over the 20th and 21st centuries, J Geophys Res Biogeosci, 126, 1–21, https://doi.org/10.1029/2021JG006304, 2021.
  - Liu, G., Yang, H., Xie, R., Yang, Y., Liu, W., Guo, X., Xue, J., Ming, B., Wang, K., Hou, P., and Li, S.: Genetic gains in maize yield and related traits for high-yielding cultivars released during 1980s to 2010s in China, Field Crops Res, 270, 108223, https://doi.org/10.1016/j.fcr.2021.108223, 2021.
- Lombardozzi, D. L., Lu, Y., Lawrence, P. J., Lawrence, D. M., Swenson, S., Oleson, K. W., Wieder, W. R., and Ainsworth, E. A.: Simulating Agriculture in the Community Land Model Version 5, J Geophys Res Biogeosci, 125, 1–19, https://doi.org/10.1029/2019JG005529, 2020.
  - Long, S. P.: Environmental Responses, C4 plant biology, Elsevier, 12–21, 1999.
- Ma, Y.., Dominic W., Mingsheng F., Lei Q., Rong L., and Johannes L. Global crop production increase by soil organic carbon.

  Nature Geoscience 16 (12): 1159-1165, 2023.
  - Maruyama, A. and Kuwagata, T.: Coupling land surface and crop growth models to estimate the effects of changes in the growing season on energy balance and water use of rice paddies, Agric For Meteorol, 150, 919–930, https://doi.org/10.1016/J.AGRFORMET.2010.02.011, 2010.
- Masutomi, Y.: The appropriate analytical solution for coupled leaf photosynthesis and stomatal conductance models for C3 plants, Ecol Modell, 481, 110306, https://doi.org/10.1016/j.ecolmodel.2023.110306, 2023.
  - Masutomi, Y., Ono, K., Mano, M., Maruyama, A., and Miyata, A.: A land surface model combined with a crop growth model for paddy rice (MATCRO-Rice v. 1) Part 1: Model description, Geosci Model Dev, 9, 4133–4154, https://doi.org/10.5194/gmd-9-4133-2016, 2016a.

- Masutomi, Y., Ono, K., Takimoto, T., Mano, M., Maruyama, A., and Miyata, A.: A land surface model combined with a crop growth model for paddy rice (MATCRO-Rice v. 1) Part 2: Model validation, Geosci Model Dev, 9, 4155–4167, https://doi.org/10.5194/gmd-9-4155-2016, 2016b.
  - Mori A., Doi, Y., Iizumi, T. GCPE: The global dataset of crop phenological events for agricultural and earth system modeling, Journal of Agricultural Meteorology, 79, 3, 120-129, https://doi.org/10.2480/agrmet.D-23-00004, 2023.
- Muchow, R. C.: Effect of nitrogen supply on the comparative productivity of maize and sorghum in a semi-arid tropical environment I. Leaf growth and leaf nitrogen, Field Crops Res, 18, 1–16, https://doi.org/10.1016/0378-4290(88)90055-X, 1988.
  - Muchow, R. C. and Sinclair, T. R.: Nitrogen response of leaf photosynthesis and canopy radiation use efficiency in field-grown maize and sorghum, Crop Sci, 34, 721–727, https://doi.org/10.2135/CROPSCI1994.0011183X003400030022X, 1994.
- Nagata, M., Yusara, A., Kato, T., and Masutomi, Y.: Development of global maize production model MATCRO-Maize version 1.0 (MATCRO-Maize vers.0), Zenodo [code and dataset], https://doi.org/10.5281/zenodo.14869444, 2025.

795

- Oleson, K. W., Lead, D. M. L., Bonan, G. B., Drewniak, B., Huang, M., Koven, C. D., Levis, S., Li, F., Riley, W. J., Subin, Z. M., Swenson, S. C., Thornton, P. E., Bozbiyik, A., Fisher, R., Heald, C. L., Kluzek, E., Lamarque, J.-F., Lawrence, P. J., Leung, L. R., Lipscomb, W., Muszala, S., Ricciuto, D. M., Sacks, W., Sun, Y., Tang, J., and Yang, Z.-L.: Technical Description of version 4.5 of the Community Land Model (CLM) Coordinating Lead Authors, NCAR, 2013.
- Olin, S., Lindeskog, M., Pugh, T. A. M., Schurgers, G., Wärlind, D., Mishurov, M., Zaehle, S., Stocker, B. D., Smith, B., and Arneth, A.: Soil carbon management in large-scale Earth system modelling: Implications for crop yields and nitrogen leaching, Earth System Dynamics, 6, 745–768, https://doi.org/10.5194/ESD-6-745-2015, 2015.
- Osborne, T., Slingo, J., Lawrence, D., and Wheeler, T.: Examining the interaction of growing crops with local climate using a coupled crop-climate model, J Clim, 22, 1393–1411, https://doi.org/10.1175/2008JCLI2494.1, 2009.
  - Osborne, T., Gornall, J., Hooker, J., Williams, K., Wiltshire, A., Betts, R., and Wheeler, T.: JULES-crop: a parametrisation of crops in the Joint UK Land Environment Simulator, Geosci. Model Dev, 8, 1139–1155, https://doi.org/10.5194/gmd-8-1139-2015, 2015.
- Paponov, I. A. and Engels, C.: Effect of nitrogen supply on leaf traits related to photosynthesis during grain filling in two
  maize genotypes with different N efficiency, Journal of Plant Nutrition and Soil Science, 166, 756–763,
  https://doi.org/10.1002/jpln.200320339, 2003.
  - Paponov, I. A., Sambo, P., Erley, G. S. auf'm., Presterl, T., Geiger, H. H., and Engels, C.: Grain yield and kernel weight of two maize genotypes differing in nitrogen use efficiency at various levels of nitrogen and carbohydrate availability during flowering and grain filling, Plant Soil, 272, 111–123, https://doi.org/10.1007/s11104-004-4211-7, 2005.
- Peng, B., Guan, K., Chen, M., Lawrence, D. M., Pokhrel, Y., Suyker, A., Arkebauer, T., and Lu, Y.: Improving maize growth processes in the community land model: Implementation and evaluation, Agric For Meteorol, 250–251, 64–89, https://doi.org/10.1016/j.agrformet.2017.11.012, 2018.

- Penning de Vries, F. W. T., Jansen, D. M., ten Berge, H. F. M., and Bakema, A.: Simulation of ecophysiological process of growth in several annual crops, Centre for Agricultural Publishing and Documentation (Pudoc), Wageningen, the Netherlands, 1989.
  - Portmann, F. T., Siebert, S., and Döll, P.: MIRCA2000—Global monthly irrigated and rainfed crop areas around the year 2000: A new high-resolution data set for agricultural and hydrological modeling, Global Biogeochem Cycles, 24, GB1011, https://doi.org/10.1029/2008GB003435, 2010.
- Ruane, A.C., Goldberg, R., and Chryssanthacopoulos, J. AgMIP climate forcing datasets for agricultural modeling: Merged products for gap-filling and historical climate series estimation, Agr. Forest Meteorol., 200, 233-248, doi:10.1016/j.agrformet.2014.09.016, 2015.
  - Sage, R. F.: Why C4 photosynthesis?, in: C4 plant biology, Elsevier, 3–16, 1999.

825

830

835

- Schaphoff, S., Forkel, M., Müller, C., Knauer, J., Von Bloh, W., Gerten, D., Jägermeyr, J., Lucht, W., Rammig, A., Thonicke, K., and Waha, K.: LPJmL4 A dynamic global vegetation model with managed land Part 2: Model evaluation, Geosci Model Dev, 11, 1377–1403, https://doi.org/10.5194/gmd-11-1377-2018, 2018.
- Sellers, P. J., Randall, D. A., Collatz, G. J., Berry, J. A., Field, C. B., Dazlich, D. A., Zhang, C., Collelo, G. D., and Bounoua, L.: A Revised Land Surface Parameterization (SiB2) for Atmospheric GCMS. Part I: Model Formulation, J Clim, 9, 676–705, https://doi.org/10.1175/1520-0442(1996)009<0676:ARLSPF>2.0.CO;2, 1996.
- Sinclair, T. R. and Horie, T.: Leaf nitrogen, photosynthesis, and crop radiation use efficiency: a review, Crop Sci, 29, 90–98, https://doi.org/10.2135/cropsci1989.0011183X002900010023x, 1989.
- Takata, K., Emori, S., and Watanabe, T.: Development of the minimal advanced treatments of surface interaction and runoff, Glob Planet Change, 38, 209–222, https://doi.org/10.1016/S0921-8181(03)00030-4, 2003.
- Tsvetsinskaya, E. A., Mearns, L. O., and Easterling, W. E.: Investigating the effect of seasonal plant growth and development in three-dimensional atmospheric simulations. part ii: atmospheric response to crop growth and development, J Clim, 14, 711–729, https://doi.org/10.1175/1520-0442(2001)014<0711:ITEOSP>2.0.CO;2, 2001.
- Tubiello, F. N. and Ewert, F.: Simulating the effects of elevated CO<sub>2</sub> on crops: approaches and applications for climate change, European Journal of Agronomy, 18, 57–74, https://doi.org/10.1016/S1161-0301(02)00097-7, 2002.
- Volkholz, J. and Müller, C.: ISIMIP3 soil input data (v1.0). ISIMIP Repository., https://doi.org/10.48364/ISIMIP.942125, 2020.
- 840 Volkholz, J. and Ostberg, S.: ISIMIP3a N-fertilizer input data (v1.2). ISIMIP Repository., https://doi.org/10.48364/ISIMIP.311496.2, 2022.
  - Vos, J., Van Der Putten, P. E. L., and Birch, C. J.: Effect of nitrogen supply on leaf appearance, leaf growth, leaf nitrogen economy and photosynthetic capacity in maize (Zea mays L.), Field Crops Res, 93, 64–73, https://doi.org/10.1016/J.FCR.2004.09.013, 2005.
- Wu, X., Vuichard, N., Ciais, P., Viovy, N., De Noblet-Ducoudré, N., Wang, X., Magliulo, V., Wattenbach, M., Vitale, L., Di Tommasi, P., Moors, E. J., Jans, W., Elbers, J., Ceschia, E., Tallec, T., Bernhofer, C., Grünwald, T., Moureaux, C., Manise,

- T., Ligne, A., Cellier, P., Loubet, B., Larmanou, E., and Ripoche, D.: ORCHIDEE-CROP (v0), a new process-based agroland surface model: Model description and evaluation over Europe, Geosci Model Dev, 9, 857–873, https://doi.org/10.5194/gmd-9-857-2016, 2016.
- Yusara, A., Kato, T., Ainsworth, E. A., Battisti, R., Kumagai, E., Nakano, S., Wu, Y., Tsutsumi-Morita, Y., Kobayashi, K., and Masutomi, Y.: Developing an eco-physiological process-based model of soybean growth and yield (MATCRO-Soy v.1): Model calibration and evaluation, EGUsphere[preprint], https://doi.org/10.5194/egusphere-2025-453, 2025.